Table 2. Tumorigenic Capacity of Unsorted, EpCAM$^+$, EpCAM$^-$, CD90$^+$, and CD90$^-$ Cells From Primary HCCs and Xenografts

Sample	CD133 (%)	CD90 (%)	EpCAM (%)	Cell Surface Marker	Number of Cells	Tumor Formation 2M	Tumor Formation 3M
P1	0	3.1	0	Unsorted	1×10^7	0/5	0/5
				CD90$^+$	1×10^5	0/5	0/5
				CD90$^-$	1×10^5	0/5	0/5
P2	0.06	7.0	0.06	Unsorted	1×10^7	0/5	0/5
				CD90$^+$	1×10^5	0/5	0/5
				CD90$^-$	1×10^5	0/5	0/5
P3	0	1.3	0	Unsorted	1×10^6	0/2	0/2
				CD90$^+$	1×10^4	0/4	0/4
				CD90$^-$	1×10^4	0/4	0/4
P4	0	0.6	17.5	Unsorted	1×10^6	3/4	4/4
				EpCAM$^+$	1×10^3	0/3	2/3
					1×10^4	3/4	4/4
					1×10^5	3/3	3/3
				CD90$^+$	1×10^3	0/3	0/3
					1×10^4	0/4	0/4
					1×10^5	0/3	0/3
				EpCAM$^-$ CD90$^-$	1×10^3	0/3	0/3
					1×10^4	0/4	0/4
					1×10^5	0/3	0/3
P5	0	0.8	29.7	Unsorted	1×10^6	0/5	0/5
				EpCAM$^+$	1×10^5	0/5	0/5
				CD90$^+$	1×10^5	0/5	0/5
				EpCAM$^-$ CD90$^-$	1×10^5	0/5	0/5
P6	0	0.7	0	Unsorted	1×10^6	0/2	0/2
				CD90$^+$	1×10^4	0/4	0/4
				CD90$^-$	1×10^4	0/4	0/4
P7	1.38	4.5	4.4	Unsorted	1×10^6	2/2	2/2
				EpCAM$^+$	2×10^2	0/3	0/3
					1×10^3	0/3	1/3
					1×10^4	2/4	4/4
				CD90$^+$	2×10^2	0/3	0/3
					1×10^3	0/3	0/3
					1×10^4	0/4	0/4
				EpCAM$^-$ CD90$^-$	1×10^3	0/3	0/3
					1×10^4	0/3	0/3
					1×10^5	0/4	0/4
P8	0	0.08	0	Unsorted	1×10^5	0/4	0/4
				CD90$^+$	1×10^3	0/3	0/3
				CD90$^-$	1×10^5	0/3	0/3
P9	0	0.26	0	Unsorted	1×10^5	0/4	0/4
				CD90$^+$	1×10^3	0/3	0/3
				CD90$^-$	1×10^5	0/3	0/3
P10	0	0.78	0	Unsorted	1×10^4	0/4	0/4
				CD90$^+$	1×10^3	0/3	0/3
				CD90$^-$	1×10^4	0/3	0/3
P11	0	0.1	1.54	Unsorted	5×10^4	0/2	0/2
				EpCAM$^+$	1×10^3	0/3	0/3
				CD90$^+$	1×10^3	0/3	0/3
				EpCAM$^-$ CD90$^-$	1×10^4	0/3	0/3
P12	0.06	0.05	0.09	Unsorted	1×10^5	0/3	3/3
				CD90$^+$	1×10^3	0/4	1/4
				CD90$^-$	1×10^3	0/4	1/4
					1×10^4	0/3	3/3
P13	0	0.03	67.7	EpCAM$^+$	5×10^5	4/4	NA
					5×10^4	3/3	NA
					5×10^3	3/3	NA
				EpCAM$^-$	5×10^5	0/4	NA
					5×10^4	0/3	NA
					5×10^3	0/3	NA
P14	24.0	0.06	3.1	EpCAM$^+$	5×10^3	4/5	NA
				EpCAM$^-$	5×10^3	2/5	NA
P15	0	2.45	0	CD90$^+$	5×10^4	3/4	NA
					5×10^3	1/3	NA
					5×10^2	1/3	NA
				CD90$^-$	5×10^4	2/4	NA
					5×10^3	1/3	NA
					5×10^2	0/3	NA

NA, not available.

contained definite CD133$^+$ cells (20%) (Table 2). CD90$^+$ cells were detected at variable frequencies in all 15 HCCs analyzed.

To explore the status of these CSC marker-positive cells in HCC in a large cohort, we utilized oligo-DNA microarray data from 238 HCC cases (GEO accession no.: GSE5975) to evaluate the expression of *EPCAM* (encoding EpCAM and CD326), *THY1* (encoding CD90), and *PROM1* (encoding CD133) in whole HCC tissues and nontumor (NT) tissues. Because previous studies demonstrated that CD133$^+$ and CD90$^+$ cells were detected at low frequency (~13.6% by CD133 staining and ~6.2% by CD90 staining) in HCC, but were almost nonexistent in NT liver (4, 5),[4,5] we utilized tumor/nontumor (T/N) gene-expression ratios to detect the existence of marker-positive CSCs in tumor. Accordingly, we showed that a 2-fold cutoff of T/N ratios of *EPCAM* successfully stratifies HCC samples with EpCAM$^+$ liver CSCs.[9,10]

A total of 95 (39.9%), 110 (46.2%), and 31 (13.0%) of the 238 HCC cases were thus regarded as EpCAM$^+$, CD90$^+$, and CD133$^+$ HCCs (T/N ratios: $\geq$2.0), respectively. As observed in the FACS data described above, we detected coexpression of EpCAM and CD90 in 45 HCCs (18.9%), EpCAM and CD133 in five HCCs (2%), CD90 and CD133 in five HCCs (2%), and EpCAM, CD90, and CD133 in 11 HCCs (4.6%). To clarify the characteristics of gene-expression signatures specific to stem cell marker expression status, we selected 172 HCC cases expressing a single CSC marker (34 EpCAM$^+$ CD90$^-$ CD133$^-$, 49 EpCAM$^-$ CD90$^+$ CD133$^-$, and 10 EpCAM$^-$ CD90$^-$ CD133$^+$) or all marker-negative HCCs (79 EpCAM$^-$ CD90$^-$ CD133$^-$). A class-comparison analysis with

univariate F tests and a global permutation test (×10,000) yielded a total of 1,561 differentially expressed genes. Multidimensional scaling (MDS) analysis using this gene set indicated that HCC specimens were clustered in specific groups with statistical significance ($P < 0.001$). Close examination of MDS plots revealed three major HCC subtype clusters: all marker-negative HCCs (blue spheres); EpCAM single-positive HCCs (red spheres); and CD90 single-positive HCCs (light blue spheres). $CD133^+$ HCCs (orange spheres) were rare, relatively scattered, and not clustered (Fig. 1B).

We examined the expression of representative hepatic stem/progenitor cell markers *AFP*, *KRT19*, and *DLK1* in HCCs with regard to the gene-expression status of each CSC marker (Fig. 1C). All three markers were up-regulated in $EpCAM^+$ and $CD133^+$ HCCs, compared with all marker-negative HCCs, consistent with previous findings.[10,11] However, we found no significant overexpression of *AFP*, *KRT19*, and *DLK1* in $CD90^+$ and all marker-negative HCCs.

Hierarchical cluster analyses revealed three main gene clusters that were up-regulated in $EpCAM^+$ HCCs (cluster A, 706 genes), $EpCAM^+$ or $CD133^+$ HCCs (cluster B, 530 genes), and $CD90^+$ or $CD133^+$ HCCs (cluster C, 325 genes) (Fig. 1D). Pathway analysis indicated that the enriched genes in cluster A (red bar) were associated with chromatin modification, cell-cycle regulation, and Wnt/β-catenin signaling (Fig. 1E). Genes associated with messenger RNA processing were enriched in clusters A (red bar) and B (orange bar). Surprisingly, genes in cluster C were significantly associated with pathways involved in blood-vessel morphogenesis, angiogenesis, neurogenesis, and epithelial mesenchymal transition (EMT) (light blue bar). Close examination of genes in each cluster suggested that known hepatic transcription factors (*FOXA1*), Wnt regulators (*TCF7L2* and *DKK1*), and a hepatic stem cell marker (*CD24*) were dominantly up-regulated in $EpCAM^+$ and $CD133^+$ HCCs (Fig. 1F). By contrast, genes associated with blood-vessel morphogenesis (*TIE1* and *FLT1*), EMT (*TGFB1*), and neurogenesis (*NES*) were activated dominantly in $CD90^+$ HCCs and $CD133^+$ HCCs.

$CD90^+$ HCC Cells Share Features With Mesenchymal Vascular Endothelial Cells. Because $CD133^+$ HCCs were relatively rare and constituted only 13% (microarray cohort) to 20% (FACS cohort) of all HCC samples analyzed, we focused on the characterization of EpCAM and CD90. To clarify the cell identity of $EpCAM^+$ or $CD90^+$ cells in primary HCCs, we performed IHC analysis of 18 needle-biopsy specimens of premalignant dysplastic nodules (DNs), 102 surgically resected HCCs, and corresponding NT liver tissues. When examining the expression of EpCAM and CD90 in cirrhotic liver tissue by double-color IHC analysis, we found that $EpCAM^+$ cells and $CD90^+$ cells were distinctively located and not colocalized (Supporting Fig. 1A). Immunoreactivity (IR) to anti-CD90 antibodies (Abs) was detected in vascular endothelial cells (VECs), inflammatory cells, fibroblasts, and neurons, but not in hepatocytes or cholangiocytes, in the cirrhotic liver (Supporting Fig. 1B, panels a,b). IR to anti-EpCAM Abs was detected in hepatic progenitors adjacent to the periportal area and bile duct epithelial cells in liver cirrhosis (Supporting Fig. 1B, panels c,d).

IR to anti-EpCAM Abs was detected in 37 of 102 surgically resected HCCs (Fig. 2A, panel b), but not in 18 DNs (Fig. 2A, panel a). By contrast, no tumor epithelial cells (TECs) showing IR to anti-CD90 Abs were found in any of the 18 DNs or 102 HCCs examined (Fig. 2A, panels c,d). However, we identified $CD90^+$ cells that were morphologically similar to VECs or fibroblasts within the tumor nodule in 37 of the 102 surgically resected HCC tissues (≥5% positive staining in a given area). IR to anti-CD90 Abs was also detected in hepatic mesenchymal tumors (Supporting Fig. 1C, panels a-c), indicating that CD90 is also a marker of liver stromal tumors.

Double-color IHC and immunofluorescence (IF) analysis confirmed the distinct expression of EpCAM and CD90 in HCC (Fig. 2B), consistent with the FACS data (Fig. 1A). Quantitative real-time polymerase chain reaction (qPCR) analysis of sorted $EpCAM^+$, $CD90^+$, and $EpCAM^-$ $CD90^-$ cells after $CD45^+$ cell depletion indicated that the hepatic stem/progenitor markers, *AFP* and *KRT19*, were up-regulated in $EpCAM^+$ cells (red bar), whereas the mesenchymal markers, *KIT* and *FLT1*, were up-regulated in $CD90^+$ cells (orange bar), compared with $EpCAM^-$ $CD90^-$ cells (blue bar) (Fig. 2C). The hepatocyte marker, *CYP3A4*, was down-regulated in $EpCAM^+$ cells and not detected in $CD90^+$ cells, compared with $EpCAM^-$ $CD90^-$ cells. *POU5F1* and *BMI1* were equally up-regulated in both $EpCAM^+$ and $CD90^+$ cells, compared with $EpCAM^-$ $CD90^-$ cells.

EpCAM and CD90 were independently and distinctively expressed in different cellular lineages, so we evaluated the staining of EpCAM and CD90 separately and analyzed the clinicopathological characteristics of surgically resected HCC cases. HCCs were regarded marker positive if ≥5% positive staining was detected in a given area. The existence of $EpCAM^+$

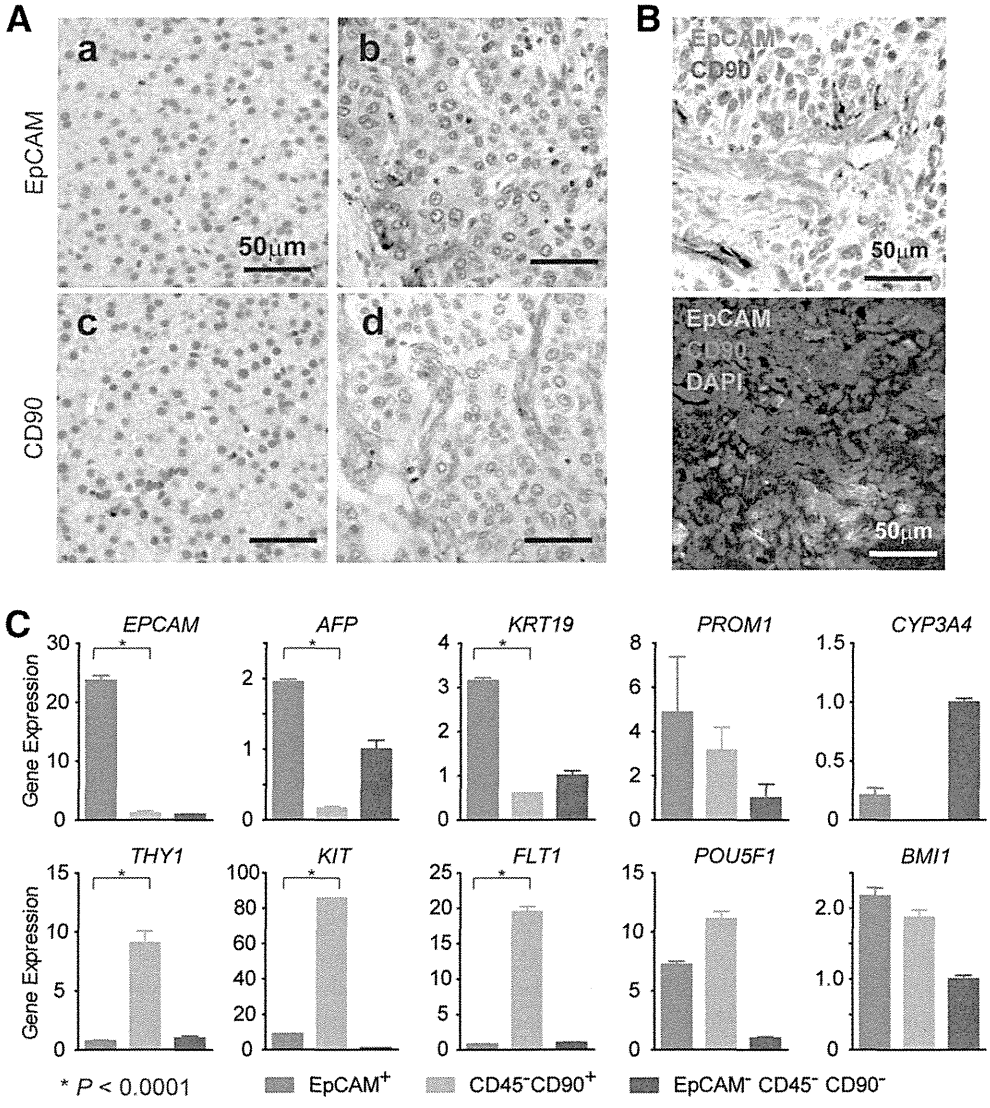

Fig. 2. Distinct EpCAM$^+$ and CD90$^+$ cell populations in HCC. (A) Representative images of EpCAM and CD90 staining in dysplastic nodule (panels a,c) and HCC (panels b,d) by IHC analysis (scale bar, 50 μm). EpCAM (panels a,b) and CD90 (panels c,d) immunostaining is depicted. (B) Upper panel: representative images of EpCAM (red) and CD90 (brown) double staining in HCC by IHC (scale bar, 50 μm). Lower panel: representative images of EpCAM (green) and CD90 (red) staining with 4'6-diamidino-phenylindole (DAPI) (blue) in HCC by IF (scale bar, 50 μm). (C) qPCR analysis of sorted EpCAM$^+$ (red bar), CD90$^+$ (orange bar), or EpCAM$^-$ CD90$^-$ (blue bar) derived from a representative primary HCC. Experiments were performed in triplicate, and data are shown as mean ± standard error of the mean.

cells (≥5%) was characterized by poorly differentiated morphology and high serum AFP values with a tendency for portal vein invasion, whereas the existence of CD90$^+$ cells (≥5%) was associated with poorly differentiated morphology and a tendency for large tumor size (Supporting Tables 2 and 3). Notably, the existence of CD90$^+$ cells was associated with a high incidence of distant organ metastasis, including lung, bone, and adrenal gland, within 2 years after surgery, whereas EpCAM$^+$ cell abundance appeared unrelated to distant organ metastasis.

We evaluated the characteristics of EpCAM$^+$ or CD90$^+$ cells in seven representative HCC cell lines. Morphologically, all EpCAM$^+$ cell lines (HuH1, HuH7, and Hep3B) showed a polygonal, epithelial cell shape, whereas three of four CD90$^+$ cell lines (HLE, HLF, and SK-Hep-1) showed a spindle cell shape (Fig. 3A). EpCAM$^+$ cells were detected in 11.5%, 57.7%, and 99.6% of sorted HuH1, HuH7, and Hep3B cells, respectively. A small CD90$^+$ cell population (0.66%) was observed in PLC/PRL/5, whereas 91.3%, 10.8%, and 59.0% of CD90$^+$ cells were detected in HLE, HLF, and SK-Hep-1, respectively. Compared with primary HCCs, only EpCAM$^+$ or CD90$^+$ cells were detected in liver cancer cell lines under normal culture conditions (Fig. 3B), suggesting that these cell lines contain a relatively pure cell population most likely obtained by clonal selection through the establishment process.

A class-comparison analysis with univariate t tests and a global permutation test (×10,000) of microarray data yielded two main gene clusters up-regulated in EpCAM$^+$ cell lines (HuH1, HuH7, and Hep3B) (cluster I, 524 genes) or in CD90$^+$ cell lines (HLE, HLF, and SK-Hep-1) (cluster II, 366 genes) (Fig. 3C). PLC/PRL/5 showed intermediate gene-expression patterns between EpCAM$^+$ and CD90$^+$ cell lines using this gene set. Pathway analysis indicated that the genes

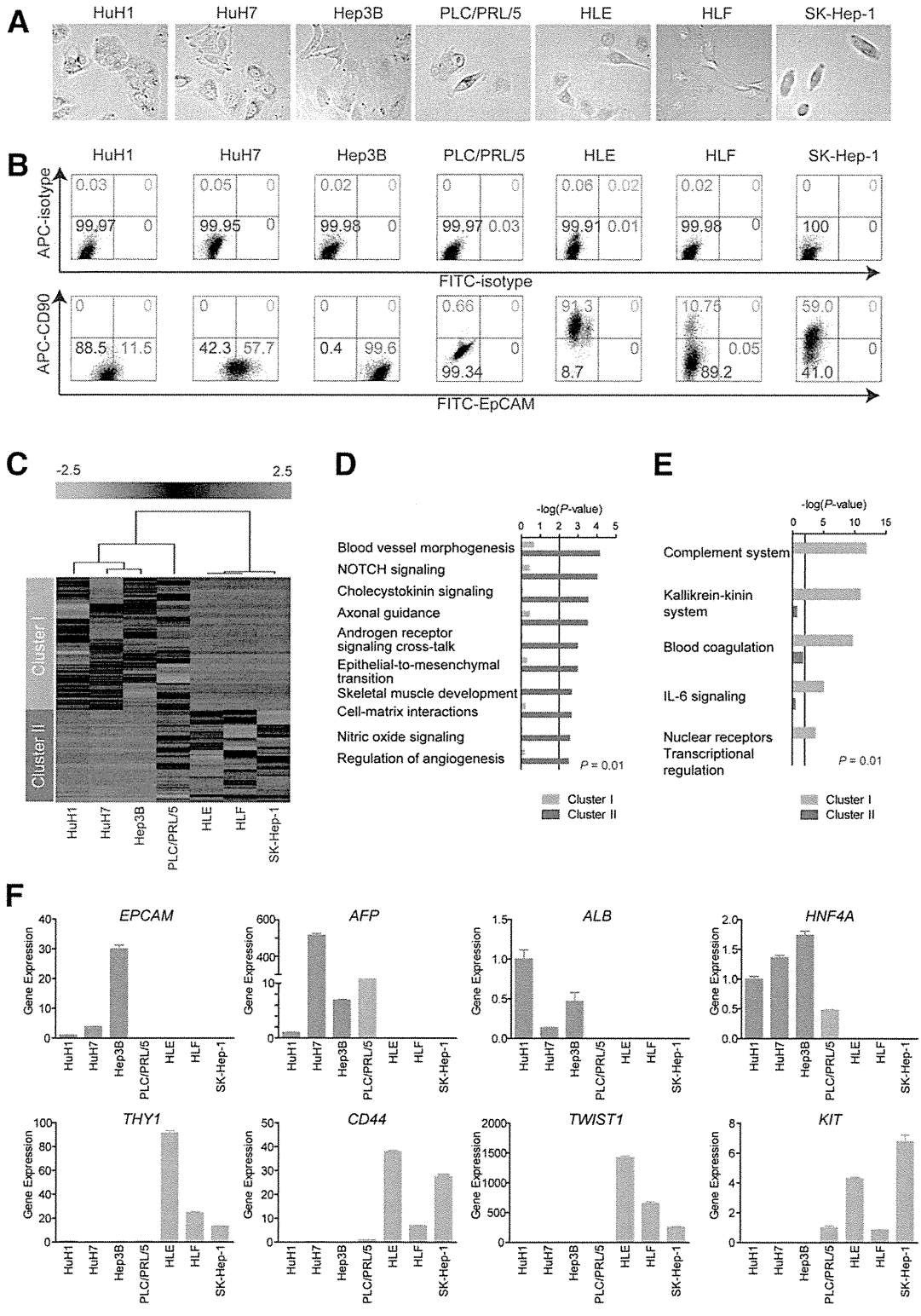

Fig. 3. Characteristics of HCC cell lines defined by EpCAM and CD90. (A) Representative photomicrographs of EpCAM^{+}CD90^{-} and EpCAM^{-} CD90^{+} HCC cell lines. (B) Representative FACS data of EpCAM^{+}CD90^{-} and EpCAM^{-} CD90^{+} HCC cell lines stained with fluorescein isothiocyanate (FITC)-EpCAM and APC-CD90 Abs. (C) Heat-map images of seven HCC cell lines based on 890 EpCAM/CD90-coregulated genes. Each cell in the matrix represents the expression level of a gene in an individual sample. Red and green cells depict high and low expression levels, respectively, as indicated by the scale bar. (D and E) Pathway analysis of EpCAM/CD90-coregulated genes. Canonical signaling pathways activated in cluster I (orange bar) or II (blue bar) with statistical significance ($P < 0.01$) are shown. (F) qPCR of representative differentially expressed genes identified by microarray analysis (C) in seven HCC cell lines.

enriched in cluster II were mainly associated with blood-vessel morpho- and angiogenesis (Fig. 3D). By contrast, the enriched genes in cluster I were significantly associated with known hepatocyte functions ($P < 0.01$) (Fig. 3E). In addition, we identified that the enriched genes in cluster II were significantly associated with neurogenesis, skeletal muscle development, and EMT.

We used qPCR to validate that known hepatic stem cell (HSC) and hepatocyte markers, such as *AFP, EPCAM, ALB*, and *HNF4A* genes, were up-regulated in $EpCAM^+$ cell lines, but not detected in $CD90^+$ cell lines (Fig. 3F). By contrast, genes associated with mesenchymal lineages and EMT, such as *KIT, TWIST1, CD44*, and *THY1*, were strongly up-regulated in $CD90^+$ cell lines.

Unique Tumorigenicity and Metastasis Capacity of Distinct CSCs Defined by EpCAM and CD90. We investigated the tumorigenic capacity of $EpCAM^+$ or $CD90^+$ cells by subcutaneously (SC) injecting 1×10^5 sorted cells of four HCC cell lines (HuH1, HuH7, HLE, and HLF) into nonobese diabetic, severe combined immunodeficient (NOD/SCID) mice. We excluded Hep3B cells for the evaluation of tumorigenicity because almost 100% of cells were EpCAM positive. We further excluded SK-Hep-1 cells from the analysis because they potentially originated from endothelial cells.[12] The highly tumorigenic capacities of $EpCAM^+$ and $CD90^+$ cells were reproduced in HuH1, HuH7, and HLF cell lines, compared with marker-negative cells (Fig. 4A). However, HLE cells did not produce SC tumors, even 12 months after transplantation, in NOD/SCID mice. $EpCAM^+$ cells from HuH1 and HuH7 formed larger tumors more rapidly than $CD90^+$ cells from HLF (Fig. 4B). IHC analyses indicated that $EpCAM^+$ cells did not produce $CD90^+$ cells and *vice versa* in these cell lines *in vivo* (Fig. 4C). $CD90^+$ cells showed a high metastatic capacity, whereas $EpCAM^+$ cells showed no metastasis to the lung when SC tumor volume reached approximately 2,000 (HuH1 and HuH7) or 700 mm^3 (HLF) (Fig. 4D). The high metastatic capacity of PLC/PRL/5 cells, which contain a small population of $CD90^+$ cells, was also confirmed after SC injection into NOD/SCID mice (data not shown). $CD90^+$ cells could divide to generate both $CD90^+$ and $CD90^-$ cells, and $CD90^+$ cells showed a high capacity to invade and form spheroids with overexpression of *TWIST1* and *TWIST2*, which are known to activate EMT programs in HLF cells (Supporting Fig. 2A-D).

We next evaluated the tumorigenic/metastatic capacity of $CD45^-$ tumor cells using 12 fresh primary HCC specimens (P1-P12) that had been surgically resected (Table 2). We further evaluated the tumorigenicity of EpCAM/CD90 sorted cells obtained from xenografts derived from primary HCCs (Supporting Fig. 3A). Of these, we confirmed the tumorigenicity of cancer cells obtained from six primary HCCs after SC injection into NOD/SCID mice within 3 months after transplantation (Fig. 5A; Table 2; Supporting Fig. 3B). $EpCAM^+$ cells derived from four HCCs (P4, P7, P13, and P14) showed highly tumorigenic capacities, compared with $EpCAM^-$ cells. $CD90^+$ cells derived from two HCCs showed equal (P12) or more-tumorigenic capacities (P15), compared with $CD90^-$ cells. Tumorigenicity of $EpCAM^+$ cells was observed in three hepatitis C virus (HCV)-related HCCs and an hepatitis B virus (HBV)-related HCC, whereas tumorigenicity of $CD90^+$ cells was observed in two HBV-related HCCs (Tables 1 and 2).

Using unsorted cells, we compared the frequency of $EpCAM^+$ and $CD90^+$ cells in primary and xenograft tumors and found that $EpCAM^+$ cells remained, but $CD90^+$ cells disappeared, in secondary tumors derived from P4 or P7, whereas $EpCAM^+$ cells disappeared, but $CD90^+$ cells remained, in secondary tumors derived from P12 (Fig. 5B). Morphologically, tumorigenic $EpCAM^+$ cells showed an epithelial cell shape, whereas $CD90^+$ cells showed a mesenchymal VEC shape (Fig. 5C and Supporting Fig. 3C). FACS analysis indicated that P12 HCC cells showed abundant expression of vascular endothelial growth factor receptor (VEGFR) 1 and a vascular endothelial marker endoglin (CD105) (Fig. 5D). By contrast, P4 and P7 HCC cells did not express these vascular endothelial markers (data not shown). Lung metastasis was detected in NOD/SCID mice transplanted with P12 HCC cells, but not in mice transplanted with P4 and P7 HCC cells (Fig. 5E,F).

Taken together, these results suggest that the tumorigenic and metastatic capability of primary HCC may depend on the presence of distinct $EpCAM^+$ or $CD90^+$ CSCs. $EpCAM^+$ cells were associated with a high tumorigenic capacity with hepatic epithelial stem cell features, whereas $CD90^+$ cells were related to the metastatic propensity with VEC features.

Suppression of Lung Metastasis Mediated by $CD90^+$ CSCs by Imatinib Mesylate. We previously demonstrated that Wnt/β-catenin signaling inhibitors could successfully attenuate the tumorigenic capacity of $EpCAM^+$ CSCs in HCC.[8,10] To explore the potential molecular targets activated in $CD90^+$ CSCs, we investigated the expression of the known VEC markers, CD105, VEGFR1 (encoded by *FLT1*), and

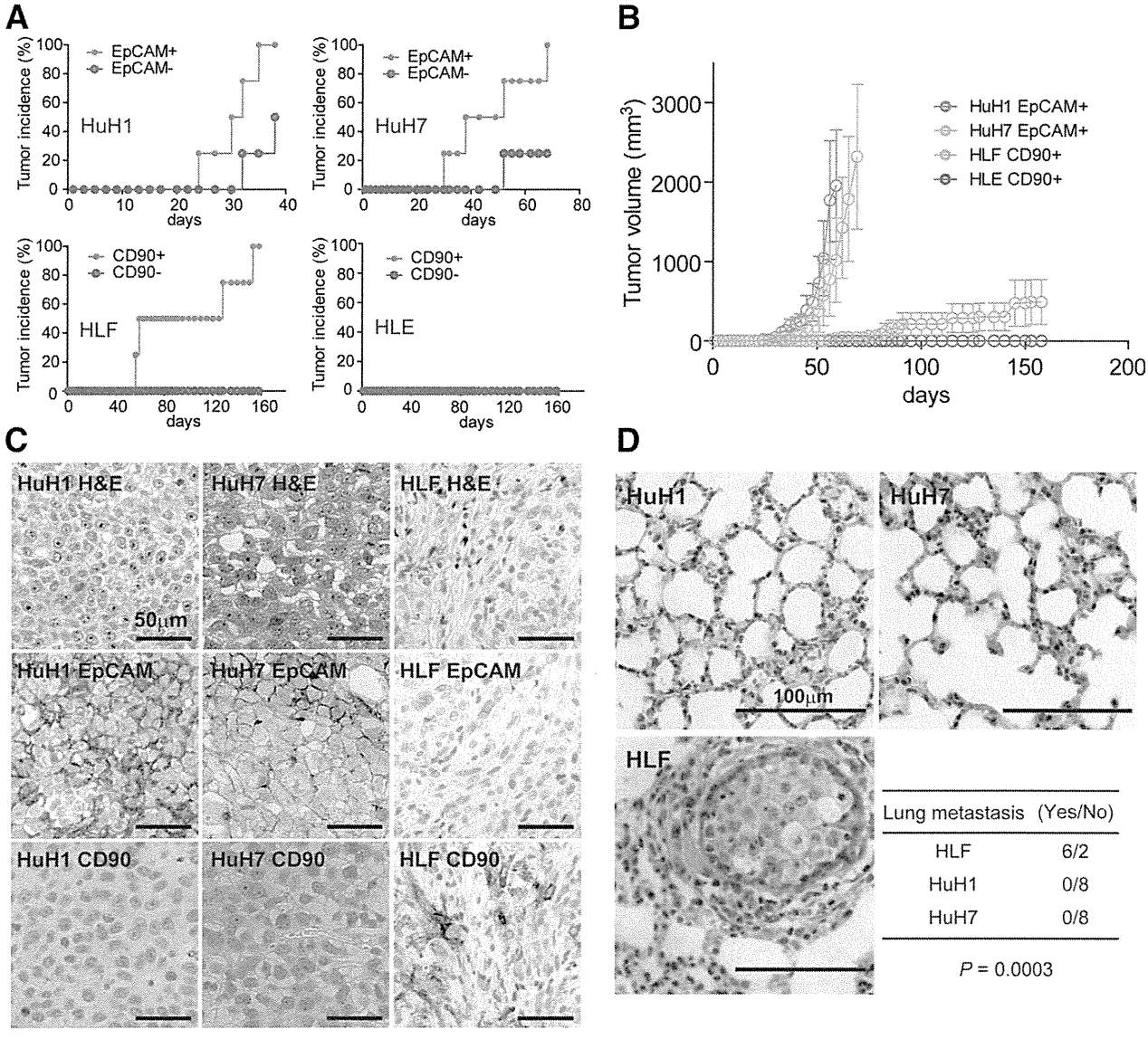

Fig. 4. Distinct tumorigenic/metastatic capacities of HCC cell lines defined by EpCAM and CD90. (A) Tumorigenicity of 1×10^5 cells sorted by anti-EpCAM (HuH1 and HuH7) or anti-CD90 (HLE and HLF) Abs. Data are generated from 8 mice/cell line. (B) Tumorigenic ability of $EpCAM^+$ and $CD90^+$ sorted cells in NOD/SCID mice. Aggressive tumor growth in the SC lesion was observed in $EpCAM^+$ HuH1 or HuH7 cells, compared with $CD90^+$ HLE or HLF cells. $EpCAM^+$ (1×10^5) or $CD90^+$ cells were injected. Tumor-volume curves are depicted as mean ± standard deviation of 4 mice/group. (C) Histological analysis of $EpCAM^+$ or $CD90^+$ cell-derived xenografts. Hematoxylin and eosin (H&E) staining of a SC tumor (upper panels) and IHC of the tumor with anti-EpCAM (middle panels) or anti-CD90 Abs (bottom panels) are shown (scale bar, 50 μm). (D) Metastasis was evaluated macroscopically and microscopically in the left and right lobes of the lung separately in each mouse (n = 4) (scale bar, 100 μm).

c-Kit (encoded by *KIT*), in cell lines and showed that they were abundantly expressed in $CD90^+$ cell lines, but not $EpCAM^+$ cell lines (Fig. 6A). No expression of VEGFR2 was detected in this set of cell lines, suggesting that molecular reagents specifically targeting VEGFR2 may have no effects on $CD90^+$ CSCs. CD44, a stem cell marker that functionally regulates redox status and is a potential target of $CD90^+$ CSCs, was also abundantly expressed in $CD90^+$ cell lines (Supporting Fig. 4A), consistent with previous data.[5,13] No significant difference was detected in the expression of the hematopoietic marker, CD34, or ABCG2 between $EpCAM^+$ and $CD90^+$ cell lines (Supporting Fig. 4A).

Among these molecular targets, we focused on the characterization of c-Kit because the c-Kit tyrosine kinase inhibitor, imatinib mesylate, is readily available, is widely used for the treatment of gastrointestinal stromal tumor with activation of c-Kit, and may have potential antitumor activity against a subset of HCC.[14] We explored the effect of imatinib mesylate on HCC cell lines and found that treatment with 10

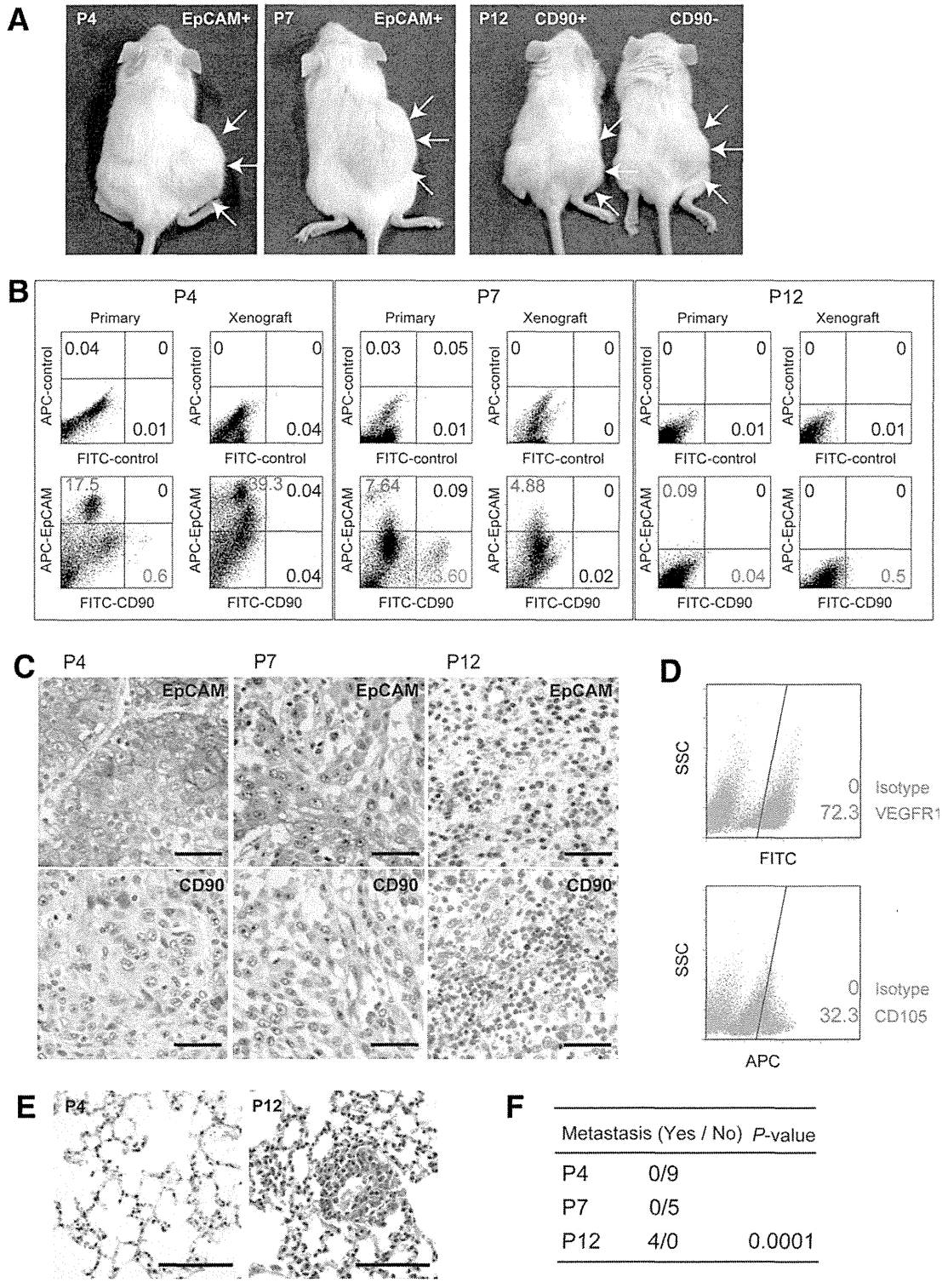

Fig. 5. Tumorigenic/metastatic capacities of EpCAM$^+$ and CD90$^+$ cells in primary HCC. (A) Representative NOD/SCID mice with SC tumors (white arrows) from EpCAM$^+$ P4 or P7 cells (left and middle panels) and CD90$^+$ or CD90$^-$ P12 cells (right panel). (B) FACS analysis of CD90 and EpCAM staining in primary HCCs and the corresponding secondary tumors developed in NOD/SCID mice. Unsorted cells (1×10^6 cells in P4 and P7 or 1×10^5 cells in P12) were SC injected to evaluate the frequency of each marker-positive cell in primary and secondary tumors. (C) IHC analysis of EpCAM and CD90 in primary HCCs P4, P7, and P12 (scale bar, 50 μm). (D) FACS analysis of VEGFR1 (Alexa488) and CD105 (APC) in primary HCC P12. (E) Hematoxylin and eosin staining of lung tissues in P4 and P12 (scale bar, 200 μm). (F) Frequency of lung metastasis in NOD/SCID mice SC transplanted using unsorted primary HCC cells.

μM reduced cell proliferation and spheroid formation in CD90$^+$ cell lines, but had no effect on EpCAM$^+$ cell lines (Supporting Fig. S4B,C).

We further explored the effect of imatinib mesylate *in vivo*. Because EpCAM$^+$ and CD90$^+$ cells reside in the primary HCC, but not in established cell lines, we SC injected HuH7 and HLF cell lines to generate tumors organized by EpCAM$^+$ and CD90$^+$ CSCs. Interestingly, when HLF cells were coinjected with HuH7 cells, EpCAM$^+$ cells could metastasize to the lung, whereas

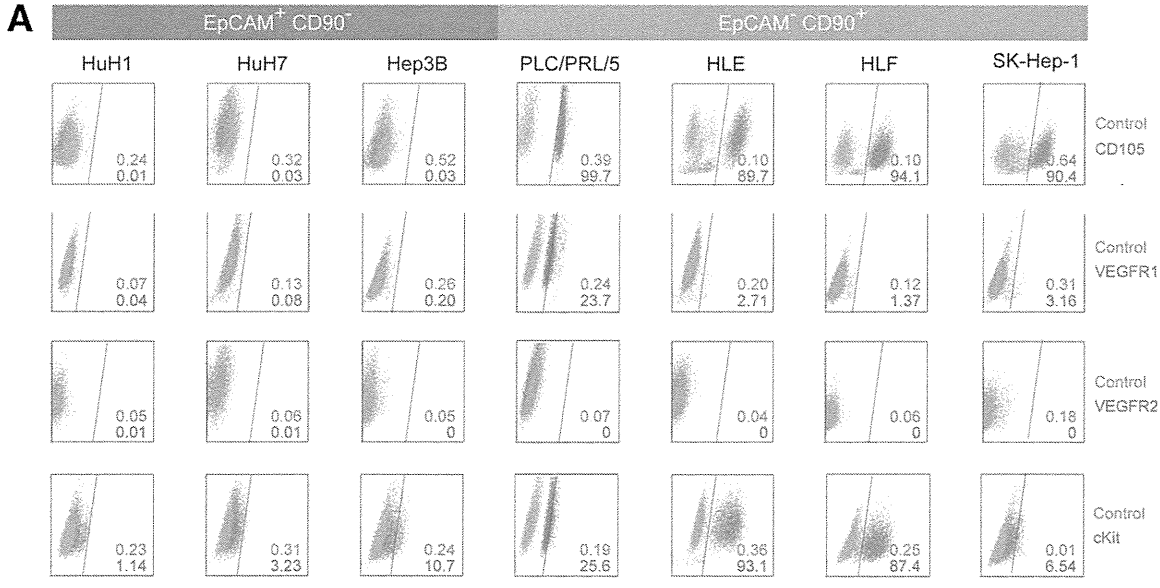

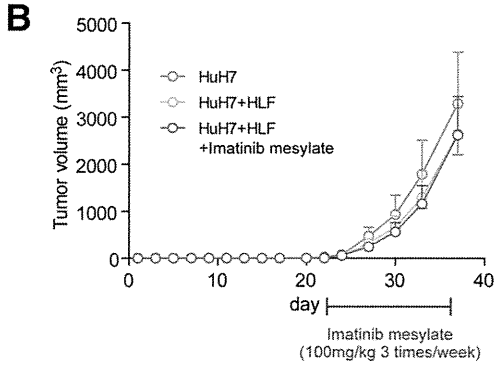

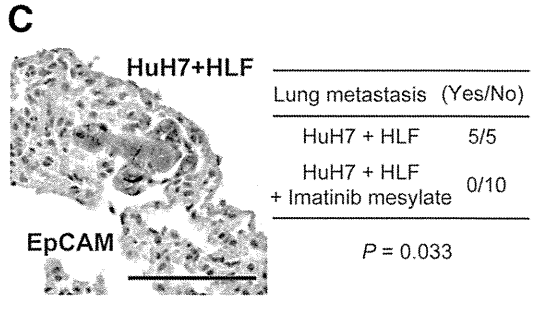

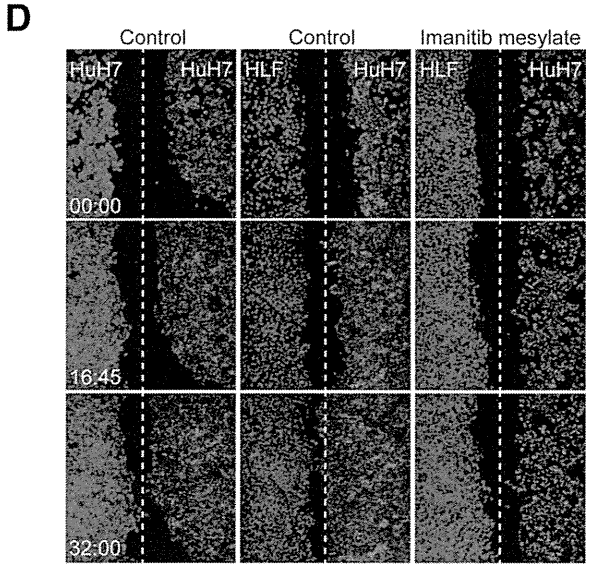

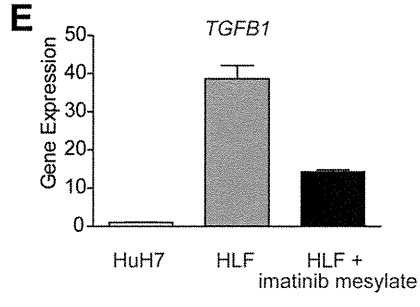

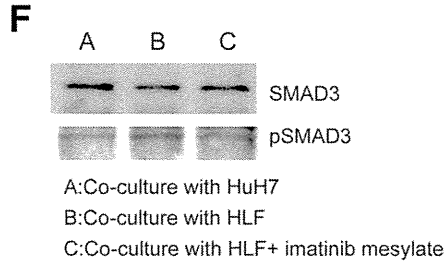

SC primary tumors showed no difference in size (Fig. 6B,C). Furthermore, although imatinib mesylate treatment had little effect on the size of primary SC tumors, it significantly suppressed lung metastasis in primary tumors (Fig. 6C). These data suggest that $CD90^+$ cells are not only metastatic to the distant organ, but also help the metastasis of $CD90^-$ cells, including $EpCAM^+$ cells, which originally have no distant metastatic capacity. Our data further suggest that imatinib mesylate can inhibit distant organ metastasis by suppressing $CD90^+$ metastatic CSCs, albeit with little effect on $EpCAM^+$ tumorigenic epithelial stem-like CSCs.

To explore the potential mechanism of how $CD90^+$ cells dictate the metastasis of $EpCAM^+$ cells, we utilized coculture systems and time-lapse image analysis. Wound-healing analysis clearly indicated that motility of HuH7 cells was enhanced when HLF cells were cocultured, and this effect was abolished by imatinib mesylate treatment (Fig. 6D; see Supporting Videos 1-3). HLF cells abundantly expressed *TGFB1*, compared with HuH7 cells, and its expression was dramatically suppressed by imatinib mesylate treatment (Fig. 6E). Mothers against decapentaplegic homolog 3 (Smad3) phosphorylation was augmented in HuH7 cells when cocultured with HLF cells, and this effect was attenuated when cocultured with HLF cells pretreated with imatinib mesylate.

Taken together, our data suggest that liver CSCs are not a single entity. Liver CSCs defined by different markers show unique features of tumorigenicity/metastasis with phenotypes closely associated with committed liver lineages. These distinct CSCs may collaborate to enhance tumorigenicity and metastasis of HCCs.

Discussion

The current investigation demonstrates that CSC marker expression status may be a key determinant of cancer phenotypes, in terms of metastatic propensity and chemosensitivity, to certain molecularly targeted therapies. EpCAM appears to be an epithelial tumorigenic CSC marker, whereas CD90 seems to be a mesenchymal metastatic CSC marker associated with expression of c-Kit and chemosensitivity to imatinib mesylate. Imatinib mesylate may be effective in inhibiting metastasis, but has little effect on primary $EpCAM^+$ HCC cell growth.

We investigated the frequency of three CSC markers (EpCAM, CD90, and CD133) in 15 primary HCCs with a confirmed cell viability of $\geq$70% and found that three HCCs contained $CD133^+$ cells, seven HCCs contained $EpCAM^+$ cells, and all HCCs contained $CD90^+$ cells. Among them, we confirmed the perpetuation of $CD133^+$ cells derived from three HCCs (P7, P12, and P14; data not shown), $EpCAM^+$ cells derived from four HCCs (P4, P7, P13, and P14), and $CD90^+$ cells derived from two HCCs (P12 and P15). Recent studies showed that at least 8 of 21 HCCs (38%)[4] and 13 of 13 HCCs (100%)[5] contained tumorigenic $CD133^+$ or $CD90^+$ CSCs, respectively. Recent IHC and tissue microarray studies also demonstrated that $CD133^+$ and $CD90^+$ cells were detected in 24.8% ($\geq$1% of tumor cells) and 32.2% ($\geq$5% of tumor cells) of HCC cases examined, respectively.[15,16]

One possible explanation of the comparatively low frequency of $CD133^+$ liver CSCs identified in our study is that we used the monoclonal Ab CD133/2, whereas Ma et al. used CD133/1. Another possible explanation is the difference of etiology related to hepatocarcinogenesis. We examined tumorigenicity using 15 HCCs (five HBV related, four HCV related, three non-B, non-C hepatitis [NBNC] related, and three alcohol related) and identified that tumorigenic CSCs were only obtained from HBV- or HCV-related cases. Previous liver CSC studies were performed using HBV-related HCCs,[4,5] and a recent study showed that

Fig. 6. Suppression of lung metastasis mediated by $CD90^+$ CSCs by imatinib mesylate. (A) FACS analysis of seven HCC cell lines stained by APC-CD105, Alexa 488/VEGFR1, APC/VEGFR2, and Alexa 488/c-Kit Abs or isotype control. (B) Tumorigenicity of 5×10^5 HuH7 cells and 2.5×10^5 HuH7 cells plus 2.5×10^5 HLF cells treated with imatinib mesylate or control phosphate-buffered saline (PBS) (200 μL/mouse) orally ingested three times per week (100 mg/kg) for 2 weeks. Data are generated from 5 mice per condition. (C) IHC analysis of EpCAM in lung metastasis detected in NOD/SCID mice SC injected with 2.5×10^5 HuH7 cells and 2.5×10^5 HLF cells. Metastasis was evaluated macro- and microscopically in the left and right lobes of the lung separately in each mouse ($n = 5$) (scale bar, 100 μm). (D) Cell motility of HuH7 cells cocultured with HuH7, HLF, or HLF cells with imatinib mesylate (10 μM) was monitored in a real-time manner by time-lapse image analysis. HuH7 and HLF cells were labeled with the lipophilic fluorescence tracer, DiI (indicated as red) or DiD (indicated as blue), and incubated in a μ-Slide eight-well chamber overnight. Silicone inserts were detached and the culture media replaced with Dulbecco's modified Eagle's medium containing 10% fetal bovine serum, including 0.1% dimethyl sulfoxide (DMSO) (control) or 10 μM of imatinib mesylate dissolved in DMSO (final concentration 0.1%). Immediately after the medium change, cells were cultured at 37°C in 5% CO_2 and time-lapse images were captured for 72 hours. (E) qPCR analysis of *TGFB1* in HuH7 (white bar), HLF (gray bar), and HLF cells pretreated with imatinib mesylate for 24 hours. (F) Smad3 and its phosphorylation evaluated by western blotting. HuH7 cells and HLF cells were harvested in cell culture inserts and treated with DMSO (0.1%) or imatinib mesylate (10 μM) for 24 hours. Cell culture inserts were washed with PBS, cocultured with HuH7 cells for 8 hours, and then removed. HuH7 cells were lysed using radioimmunoprecipitation assay buffer for western blotting. (A) HuH7 cells cocultured with HuH7 cells. (B) HuH7 cells cocultured with HLF cells. (C) HuH7 cells cocultured with HLF cells pretreated with imatinib mesylate.

HBV X may play a role in generating $EpCAM^+$ CSCs.[17] The role of hepatitis virus infection on the generation of CSCs is still unclear and should be clarified in future studies.

We were unable to confirm the tumorigenicity of $CD90^+$ cells in 13 of 15 HCCs, but we observed abundant $CD90^+$ cells in more-advanced HCCs by IHC (data not shown). Tumorigenic $CD90^+$ cells may emerge at a later stage of hepatocarcinogenesis, and the majority of $CD90^+$ cells in early HCCs may be cancer-associated VECs without tumorigenic capacity. Furthermore, we identified tumorigenic $CD90^+$ cells only from HBV-related HCCs, and a recent study suggested that expression of CD90 was associated with HBV infection.[16] We could not detect the small population of $CD90^+$ HuH7 and Hep3B cells reported on by Yang et al. However, because we identified a small population of $CD90^+$ HuH7 cells after treatment with 5-FU (manuscript in preparation), it is conceivable that different cellular stress statuses may explain the observed differences between our findings and those of Yang et al.

The majority of CSC markers discovered thus far are almost identical to those found in healthy tissue stem cells or embryonic stem cells. However, with regard to the liver, the characteristics of healthy hepatic stem/progenitor cells isolated using different stem cell markers are currently under investigation. A recent article examined the characteristics of $EpCAM^+$ and $CD90^+$ oval cells isolated from 2-acetylaminofluorene/partial hepatectomy or D-galactosamine-treated rats.[18] Interestingly, $EpCAM^+$ and $CD90^+$ oval cells represent two distinct populations: The former expresses classical oval cell markers, such as AFP, OV-1, and cytokeratin-19 (CK-19), whereas the latter expresses desmin and alpha smooth muscle actin, but not AFP, OV-1, or CK-19, which indicates that $CD90^+$ populations are more likely to be mesenchymal cells. Another study has demonstrated that mesenchymal cells can interact with HSCs to regulate cell-fate decision.[19] We found that $EpCAM^+$ and $CD90^+$ cells isolated from liver cancer are distinct in terms of gene- and protein-expression patterns in both primary liver cancers and cell lines. Furthermore, these distinct CSCs can interact to regulate the tumorigenicity and metastasis of HCC. Molecular characteristics of $EpCAM^+/CD90^+$ CSCs may potentially reflect the cellular context of healthy stem or progenitor cells.

Although our study strongly indicates that abundant $CD90^+$ cells in a tumor is a risk for distant metastasis in liver cancer, the cell identity and role of $CD90^+$ cells remains elusive. As our IHC, FACS, and xeno-transplantation assays revealed, some $CD90^+$ cells in liver cancer may be cancer-associated VECs or fibroblasts that cannot perpetuate in the xenograft. Recent findings have suggested the importance of stromal cells in tumorigenesis and cancer metastasis,[20-22] so it is possible that these cells may help TECs invade and intravasate into blood vessels, thus playing crucial roles in metastasis.

Another possibility is that $CD90^+$ cells are cancer cells with features of fibroblasts (having undergone EMT) or VECs (having undergone vasculogenic mimicry; VM) that can invade, intravasate, and metastasize cells to distant organs. Recently, two groups reported that a subset of tumor VECs originate from glioblastoma CSCs.[23,24] We successfully confirmed the tumorigenicity and metastatic capacity of $CD90^+$ cells that were morphologically identical to VECs from primary HCCs that could perpetuate in the xenograft. However, a recent study demonstrated that $CD90^+$ HCC cells express glypican-3, a marker detected in hepatic epithelial cells.[25] Further studies are warranted to clarify the nature and role of $CD90^+$ HCC cells.

In our study, $CD90^+$ cells expressed the endothelial marker, c-Kit, CD105, and VEGFR1, and a mesenchymal VEC morphology and high metastatic capacity were confirmed in both primary liver cancer and cell lines. We further confirmed that $CD90^+$ liver cancer cells showed chemosensitivity to imatinib mesylate, suggesting that cancer cells committed to mesenchymal endothelial lineages could be eradicated by the compound. Although imatinib mesylate treatment had little effect on the size of primary tumors originated from both $EpCAM^+$ and $CD90^+$ CSCs, it significantly suppressed lung metastasis *in vivo*. These data are consistent with a recent phase II study demonstrating the tolerable toxicity, but limited efficacy, of imatinib mesylate alone for unresectable HCC patients. Eligibility of imatinib mesylate for advanced HCC patients may be restricted to the HCC subtypes organized by $CD90^+$ CSCs with a highly metastatic capacity and VEC features. Therefore, a combination of compounds targeting $EpCAM^+$ tumorigenic CSCs as well as $CD90^+$ metastatic CSCs may be required for the eradication of HCC and should be tested in the future.

Acknowledgments: The authors thank Ms. Nami Nishiyama and Ms. Mikiko Nakamura for their excellent technical assistance.

References

1. Tsai WL, Chung RT. Viral hepatocarcinogenesis. Oncogene 2010;29: 2309-2324.

2. Chiba T, Kita K, Zheng YW, Yokosuka O, Saisho H, Iwama A, et al. Side population purified from hepatocellular carcinoma cells harbors cancer stem cell-like properties. HEPATOLOGY 2006;44:240-251.
3. Haraguchi N, Ishii H, Mimori K, Tanaka F, Ohkuma M, Kim HM, et al. CD13 is a therapeutic target in human liver cancer stem cells. J Clin Invest 2010;120:3326-3339.
4. Ma S, Tang KH, Chan YP, Lee TK, Kwan PS, Castilho A, et al. miR-130b promotes CD133(+) liver tumor-initiating cell growth and self-renewal via tumor protein 53-induced nuclear protein 1. Cell Stem Cell 2010;7:694-707.
5. Yang ZF, Ho DW, Ng MN, Lau CK, Yu WC, Ngai P, et al. Significance of CD90+ cancer stem cells in human liver cancer. Cancer Cell 2008;13:153-166.
6. Zen Y, Fujii T, Yoshikawa S, Takamura H, Tani T, Ohta T, Nakanuma Y. Histological and culture studies with respect to ABCG2 expression support the existence of a cancer cell hierarchy in human hepatocellular carcinoma. Am J Pathol 2007;170:1750-1762.
7. Lee TK, Castilho A, Cheung VC, Tang KH, Ma S, Ng IO. CD24(+) liver tumor-initiating cells drive self-renewal and tumor initiation through STAT3-mediated NANOG regulation. Cell Stem Cell 2011;9: 50-63.
8. Yamashita T, Budhu A, Forgues M, Wang XW. Activation of hepatic stem cell marker EpCAM by Wnt-beta-catenin signaling in hepatocellular carcinoma. Cancer Res 2007;67:10831-10839.
9. Yamashita T, Forgues M, Wang W, Kim JW, Ye Q, Jia H, et al. EpCAM and alpha-fetoprotein expression defines novel prognostic subtypes of hepatocellular carcinoma. Cancer Res 2008;68:1451-1461.
10. Yamashita T, Ji J, Budhu A, Forgues M, Yang W, Wang HY, et al. EpCAM-positive hepatocellular carcinoma cells are tumor-initiating cells with stem/progenitor cell features. Gastroenterology 2009;136: 1012-1024.
11. Ma S, Chan KW, Hu L, Lee TK, Wo JY, Ng IO, et al. Identification and characterization of tumorigenic liver cancer stem/progenitor cells. Gastroenterology 2007;132:2542-2556.
12. Heffelfinger SC, Hawkins HH, Barrish J, Taylor L, Darlington GJ. SK HEP-1: a human cell line of endothelial origin. In Vitro Cell Dev Biol 1992;28A:136-142.
13. Ishimoto T, Nagano O, Yae T, Tamada M, Motohara T, Oshima H, et al. CD44 variant regulates redox status in cancer cells by stabilizing the xCT subunit of system xc(-) and thereby promotes tumor growth. Cancer Cell 2011;19:387-400.
14. Ramadori G, Fuzesi L, Grabbe E, Pieler T, Armbrust T. Successful treatment of hepatocellular carcinoma with the tyrosine kinase inhibitor imatinib in a patient with liver cirrhosis. Anticancer Drugs 2004;15: 405-409.
15. Kim H, Choi GH, Na DC, Ahn EY, Kim GI, Lee JE, et al. Human hepatocellular carcinomas with "Stemness"-related marker expression: keratin 19 expression and a poor prognosis. HEPATOLOGY 2011;54: 1707-1717.
16. Lu JW, Chang JG, Yeh KT, Chen RM, Tsai JJ, Hu RM. Overexpression of Thy1/CD90 in human hepatocellular carcinoma is associated with HBV infection and poor prognosis. Acta Histochem 2011;113: 833-838.
17. Arzumanyan A, Friedman T, Ng IO, Clayton MM, Lian Z, Feitelson MA. Does the hepatitis B antigen HBx promote the appearance of liver cancer stem cells? Cancer Res 2011;71:3701-3708.
18. Yovchev MI, Grozdanov PN, Zhou H, Racherla H, Guha C, Dabeva MD. Identification of adult hepatic progenitor cells capable of repopulating injured rat liver. HEPATOLOGY 2008;47:636-647.
19. Wang Y, Yao HL, Cui CB, Wauthier E, Barbier C, Costello MJ, et al. Paracrine signals from mesenchymal cell populations govern the expansion and differentiation of human hepatic stem cells to adult liver fates. HEPATOLOGY 2010;52:1443-1454.
20. Dome B, Timar J, Ladanyi A, Paku S, Renyi-Vamos F, Klepetko W, et al. Circulating endothelial cells, bone marrow-derived endothelial progenitor cells and proangiogenic hematopoietic cells in cancer: from biology to therapy. Crit Rev Oncol Hematol 2009;69:108-124.
21. Karnoub AE, Dash AB, Vo AP, Sullivan A, Brooks MW, Bell GW, et al. Mesenchymal stem cells within tumour stroma promote breast cancer metastasis. Nature 2007;449:557-563.
22. Mishra PJ, Humeniuk R, Medina DJ, Alexe G, Mesirov JP, Ganesan S, et al. Carcinoma-associated fibroblast-like differentiation of human mesenchymal stem cells. Cancer Res 2008;68:4331-4339.
23. Ricci-Vitiani L, Pallini R, Biffoni M, Todaro M, Invernici G, Cenci T, et al. Tumour vascularization via endothelial differentiation of glioblastoma stem-like cells. Nature 2010;468:824-828.
24. Wang R, Chadalavada K, Wilshire J, Kowalik U, Hovinga KE, Geber A, et al. Glioblastoma stem-like cells give rise to tumour endothelium. Nature 2010;468:829-833.
25. Ho DW, Yang ZF, Yi K, Lam CT, Ng MN, Yu WC, et al. Gene expression profiling of liver cancer stem cells by RNA-sequencing. PLoS One 2012;7:e37159.

Liver INTERNATIONAL
OFFICIAL JOURNAL OF THE INTERNATIONAL ASSOCIATION FOR THE STUDY OF THE LIVER

Liver International ISSN 1478-3223

CLINICAL STUDIES

Heterogeneous nuclear ribonucleoprotein A2/B1 in association with hTERT is a potential biomarker for hepatocellular carcinoma

Hideki Mizuno[1], Masao Honda[1,2], Takayoshi Shirasaki[1,2], Taro Yamashita[1], Tatsuya Yamashita[1], Eishiro Mizukoshi[1] and Shuichi Kaneko[1]

1 Department of Gastroenterology, Kanazawa University Graduate School of Medicine, Kanazawa, Japan
2 Department of Advanced Medical technology, Kanazawa University Graduate School of Health Medicine, Kanazawa, Japan

Keywords
HCC – hnRNP A2/B1 – hTERT

Abbreviations
HCC, hepatocellular carcinoma; hnRNP A2/B1, heterogeneous nuclear ribonucleoprotein A2/B1; hTERC, human telomerase RNA component; hTERT, human telomerase reverse transcriptase subunit; TRAP, telomere repeat amplification protocol.

Correspondence
Masao Honda, Department of Gastroenterology, Graduate School of Medicine, Kanazawa University, Takara-machi 13-1, Kanazawa 920-8641, Japan
Tel: +81 76 265 2235
Fax: +81 76 234 4250
e-mail: mhonda@m-kanazawa.jp

Received 31 August 2011
Accepted 2 February 2012

DOI:10.1111/j.1478-3231.2012.02778.x

Abstract

Background: The heterogeneous nature of hepatocellular carcinoma (HCC) and the lack of appropriate biomarkers have hampered patient prognosis and treatment stratification. To identify a new prognostic biomarker that is related to human telomerase reverse transcriptase (hTERT) in HCC, we employed a unique proteomics approach using liquid chromatograph-mass spectrometry/mass spectrometry (LC-MS/MS) after gel filtration purification of liver tissue. *Methods:* Protein lysates from HCC and cirrhotic liver tissue were subjected to gel filtration using high performance liquid chromatography. The telomerase complex was identified at a molecular mass of 350 kDa in parallel with telomerase activity. These fractionated lysates of 350 kDa were analyzed by LC-MS/MS. The relation of the identified marker and prognosis was statistically examined in surgically resected HCC patients. *Results:* We identified 24 differentially expressed proteins in HCC. One of these proteins, heterogeneous nuclear ribonucleoprotein A2/B1 (hnRNP A2/B1), was further analyzed by immunoprecipitation assay using tissue and cell line samples and found to interact with hTERT. Moreover small interfering RNA against hnRNP A2/B1 suppressed telomerase activity, and immunohistochemical examination showed that the enhanced nuclear and cytoplasmic hnRNP A2/B1 expression in HCC was significantly associated with histological grade of tumor differentiation and microvascular invasion of HCC. Furthermore, survival analysis of 74 HCC patients who received curative surgical treatment showed that hnRNP A2/B1 expression is an independent prognostic factor for patient survival. *Conclusions:* Heterogeneous nuclear ribonucleoprotein A2/B1, an hTERT-associated protein, is a potential prognostic biomarker for HCC patients and might be a therapeutic target of HCC.

Hepatocellular carcinoma (HCC) has extremely poor prognosis and remains one of the most aggressive human malignancies worldwide(1, 2). The high mortality associated with this disease can be attributed mainly to the inability to diagnose HCC patients at an early stage. Currently, α-fetoprotein (AFP) and protein induced by vitamin K absence or antagonists-II (PIVKA-II) are serologic biomarkers for HCC in clinical practice. However, the sensitivity of these markers is not adequate, and a nonspecific elevation in cirrhotic liver is frequently observed. Furthermore, there is an urgent need to identify additional diagnostic as well as prognostic biomarkers of HCC.

Telomerase is a ribonucleoprotein complex that maintains chromosome stability and cell lifespan by telomere maintenance(3–5). The minimal components of active telomerase include human telomerase reverse transcriptase (hTERT), the catalytic subunit, and its template RNA (hTERC) that encodes the template for synthesizing telomeric DNA(6, 7). Various host factors are associated with telomerase and maintain the homeostasis of telomeres(8). Although direct evaluation of protein expression of hTERT would be clinically useful, measurement of hTERT expression in tissue samples is less sensitive and unreliable due to the limitation of appropriate hTERT antibody(9). It would be ideal if some of the hTERT-associated proteins were closely linked to telomerase activity as this could function as a useful biomarker of tumor growth, invasion, and metastasis of HCC.

The aim of this study was to identify a new prognostic biomarker of HCC which was related to hTERT. By employing a proteomics approach combined with gel-filtration protein purification method, we found that the heterogeneous nuclear ribonucleoprotein (hnRNP)

A2/B1 was associated with hTERT and would be a useful prognostic marker of HCC.

Materials and methods

Tissue collection and preparation

All HCC and adjacent cirrhotic (non-cancerous) liver tissue samples were obtained from 74 patients who underwent surgical resection between 2000 and 2009 at Kanazawa University Hospital, Kanazawa, Japan. Follow-ups were terminated in February, 2011. The median follow-up was 38 months (range, 2–83 months). Follow-up data of clinical, aetiological, histological, imaging (ultrasonography, contrast-enhanced helical computed tomography, and magnetic resonance imaging), and treatment details were collected prospectively and added to a customized database as soon as an event such as surgery, follow-up, or death occurred.

Liver tissue samples were formalin-fixed, paraffin-embedded, and used for immunohistochemistry. Histological characterization of HCC and adjacent cirrhotic liver was performed according to the Classification of the Liver Cancer Study Group of Japan and the method described by Desmet *et al.*(10).

For proteomics analysis, three HCC and adjacent cirrhotic liver tissue samples were snap-frozen and stored in liquid nitrogen until later use in gel filtration. Three patients for proteomics analysis belong to the group of 74 patients who underwent surgical resection and were followed-up. The characteristics of these patients were described previously (patients Nos. 4, 8, and 10). All three were positive for Hepatitis C virus (HCV) antibody, and histological examination of HCC was moderately differentiated in two patients and poorly differentiated in one patient(11).

The study was approved by the appropriate ethics committees and the institutional review boards at Kanazawa University and complied with Good Clinical Practice Guidelines, the Declaration of Helsinki, and local laws and regulations.

Preparation of protein lysates and gel filtration of protein lysates

Hepatocellular carcinoma and adjacent cirrhotic liver tissue (100 mg) were ground into powder, homogenized in CelLytic^{TM} MT (detergent, bicine, and 150 mM NaCl; Sigma-Aldrich, St Louis, MO,USA), and sonicated. Protein lysates from the tissue specimens were independently fractionated on HiLoad 16/60 Superdex 200 pg gel filtration columns using a high-performance liquid chromatography (HPLC) system (GE Healthcare, Buckinghamshire, England, UK), which provides rapid screening, method scouting, method optimization, and scale-up experiments, in CelLytic^{TM} MT (Sigma-Aldrich). The resulting fractions were resolved by sodium dodecyl sulfate polyacrylamide gel electrophoresis (SDS-PAGE), probed with various antibodies, and used for proteomic study by liquid chromatograph-mass spectrometry/mass spectrometry (LC-MS/MS). The column was calibrated with a high molecular weight calibration kit (HMW Native Marker Kit; GE Healthcare).

Protein identification by mass spectrometry

Protein-fractionated lysates were carbamidomethylated by 6M Urea, 500 mM Tris–HCL, 2.5 mM EDTA, and 250 mM iodoacetamide and digested with 100 ng/uL trypsin. Peptide mixtures were redissolved in 0.5% trifluoroacetic acid (TFA), and 1 μg of the peptide solution was mixed with 1 μL of matrix (4-hydroxy-α-cyanocinnamic acid in 30% ACN, 0.1% TFA) before spotting on a target plate. The digested peptides were analyzed by a Hitachi Liquid Chromatograph Mass Spectrometer coupled to a Q-TOF Mass Spectrometer (NanoFrontier eLD; Hitachi High-Technologies Co. Ltd., Tokyo, Japan). The acquired MS/MS spectra were searched for in Swiss-Prot using the Mascot search engine (Matrix Sciences, London, UK). Search parameters were set as follows: peptide mass tolerance, ± 0.3 Da; MS/MS ion mass tolerance, ± 0.3 Da; and trypsin for the enzyme set. The proteins were identified using a P value of ≤ 0.05 and Mascot scores of >35 were considered as promising hits. The mean expression ratio of in HCC to proteins identified in adjacent cirrhotic liver tissue was calculated, and a difference of more than two-fold was used as a filtering criterion.

Immunoprecipitation of protein lysates

The protein lysates were incubated at 4°C for 3 h with 10 μL of GammaBind G resin containing prebound anti-FLAG M2 (Sigma–Aldrich) or anti-hnRNP A2/B1 (Abcam, Cambridge, UK), followed by three washes with CelLytic^{TM} MT (Sigma-Aldrich). These bound proteins were separated by SDS-PAGE and visualized by western blotting.

Plasmid construction

The FLAG-GST retrovirus expression vector pBabe-puro-FLAG-GST was constructed by inserting the *FbaI-XhoI* fragment of FLAG-GST cDNA into the *BamHI-SalI* site of the pBabe-puro vector. The GST cDNA of pBabe-puro-FLAG-GST was replaced by the *EcoRI-SalI* fragment containing hTERT cDNA and resulted in retrovirus delivery vector pBabe-puro-FLAG-hTERT(12).

Mammalian cell lines and retrovirus delivery

Huh7 (human hepatocellular carcinoma cell line) and 293T cells (human kidney cell line) were cultured by standard methods in Dulbecco's modified Eagle's med-

ium (DMEM; Gibco BRL, Gaithersburg, MD, USA) supplemented with 10% fetal bovine serum (FBS) and 1% penicillin/streptomycin. Recombinant retrovirus packaging, infection, and selection of FLAG-hTERT expressing stable transformations of Huh7 cells were preformed as described(13).

Preparation of cell lysates and immunoprecipitation

Cells were harvested, washed with phosphate buffered solution (-) and sonicated in CelLytic™ M (SigmaAldrich). Lysates of 5 × 10(6) cells were diluted 10-fold in CelLytic™ M and incubated at 4°C for 3 h with 10 μL of GammaBind G resin containing prebound anti-FLAG M2 or anti-hnRNP A2/B1, followed by three washes with CelLytic™ M. The bound proteins were separated by SDS-PAGE and visualized by western blotting.

Antibodies and western blot analysis

For western blot analysis, total cell lysates and their fractions from gel filtration were separated by SDS-PAGE and transferred to a nitrocellulose membrane then probed with anti-hTERT (Rockland Inc., Gilbertsville, PA, USA), anti-Hsp90α/β (Santa Cruz Biotechnology, CA, USA), anti-hnRNP A2/B1 (Abcam), anti-FLAG M2 (Sigma-Aldrich), or anti-β-actin (Sigma-Aldrich) primary antibodies, followed by incubation with horseradish peroxidase conjugated goat anti-mouse immunoglobulin (Ig) G secondary antibody (Amersham Biosciences, Buckinghamshire, England, UK) for anti-Hsp90α/β, anti-hnRNP A2/B1, anti-FLAG M2, and anti-β-actin antibodies or horseradish peroxidase conjugated goat anti-Rabbit IgG secondary antibody (Thermo Scientific, Rockford, IL, USA) for anti-hTERT antibody. Densitometric analysis was conducted directly on the blotted membrane using a CCD camera (LAS-3000 Mini; Fujifilm, Tokyo, Japan) and Scion Image software.

Small interfering RNA synthesis

Small interfering (si) RNA specific to hnRNP A2/B1 (HNRNPA2B1 siGENOME set) and the siGENOME Controls Basic kit were obtained from Thermo Scientific. To each well of a six-well plate, 2 × 10^5 Huh7 cells were seeded 12 h before transfection. Transfection was preformed using TransMessenger™ Transfection Reagent (Qiagen, West Sussex, UK) according to the manufacturer's protocol. A total of 100 pmol/L of siRNA duplex was used for each transfection.

Real-time quantitative reverse-transcription PCR

Real-time quantitative reverse-transcription polymerase chain reaction (RT-PCR) was performed for hnRNP A2/B1 using the ABI Prism 7900HT Sequence Detection System (Applied Biosystems, San Francisco, CA, USA). Primers and the TaqMan probe for hnRNP A2/B1were designed using the primer design software Primer Express™ (Applied Biosystems). The probe was labeled with a reporter fluorescent dye (6-carboxy-fluorescein) at the 5′ end and a quencher fluorescent dye (6-carboxy-tetramethyl-rhodamine) at the 3′ end. PCR conditions were 1 cycle at 50°C for 2 min and 95°C for 10 min, followed by 40 cycles at 95°C for 15 s and 60°C for 1 min. The level of messenger RNA (mRNA) expression relative to the internal control (β-actin) was calculated.

Telomerase activity assay

Telomerase activity was measured by a PCR-based telomere repeat amplification protocol (TRAP) enzyme-linked immunosorbent assay (ELISA). Telomerase activity was quantitatively measured using a TRAPEZE ELISA telomerase detection kit (MILLIPORE, Billerica, MA, USA) according to the manufacturer's protocol.

Immunohistochemical analysis

Paraffin-embedded sections of tissue blocks were orderly rehydrated to xylene and sequential alcohols, washed, and blocked by incubating slides in 0.6% hydrogen peroxide. The sections were treated with a 1:100 diluted solution of anti-hnRNP A2/B1 antibody for 30 min in a wet incubation box. Detection of the antibody was processed according to the manufacturer's protocol using Envision+ kits (Dako, Carpinteria, CA, USA). Slides were counterstained with hematoxylin for 30 s, dehydrated reversibly using sequential alcohols and xylene, and mounted with a coverslip using Histomount. Photographs for stained tissue section were captured using an Olympus DP70 CCD camera with an Olympus AX80 microscope (Olympus, New York, NY, USA).

Statistical analysis

The student's *t*-test was used to determine the statistical significance of the difference in cell viability between the two groups. The chi-square test was used to evaluate the correlation between clinicopathological characteristics and nuclear and cytoplasmic hnRNP A2/B1 expression. Univariate and multivariate Cox proportional hazards regression analysis was used to evaluate the association of nuclear and cytoplasmic hnRNP A2/B1 expression and clinicopathological parameters with patient outcome. All statistical analysis was performed using SPSS software (SPSS software package; SPSS Inc., Chicago, IL, USA).

Results

Fractionation of protein lysates from hepatocellular carcinoma and cirrhotic liver tissue

Protein lysates from HCC and cirrhotic liver tissue from patients were independently subjected to gel filtration

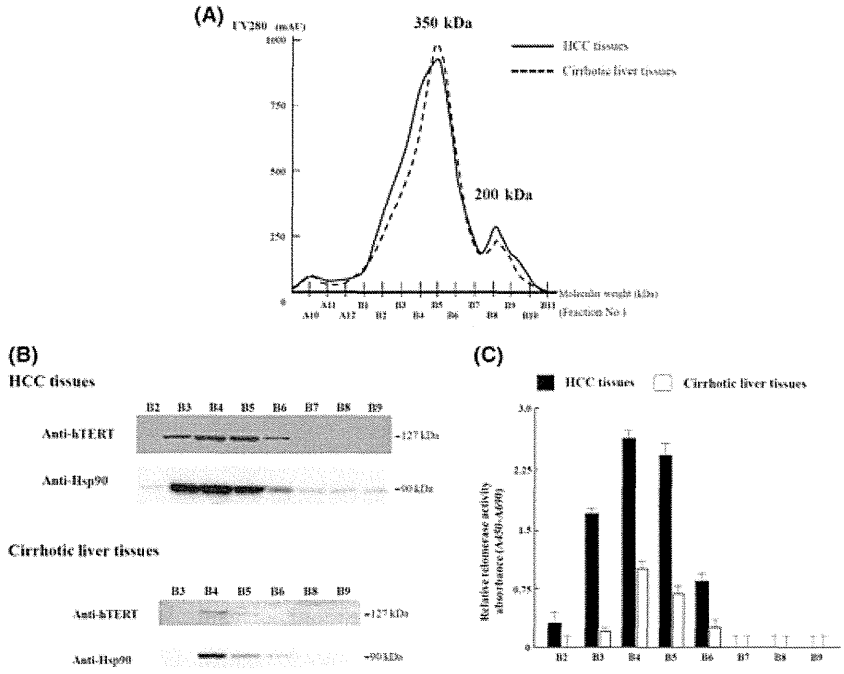

Fig. 1. Fractionation of protein lysates from HCC and cirrhotic liver tissue. (A) Protein lysates from HCC and cirrhotic liver tissues from three patients were fractionated on a 200 pg gel filtration column by high-performance liquid chromatography (HPLC). Mean values were drawn in the same axis. (B) Representative image of quantitative measurement of human telomerase reverse transcriptase (hTERT) protein and Hsp90 protein by western blotting with respective antibodies. (C) Relative telomerase activity of fractions measured by telomere repeat amplification protocol enzyme-linked immunosorbent assay.

by HPLC (Fig. 1A). Two peaks, corresponding to the molecular weights 350 kDa and 200 kDa in the fractionated proteins were found. Interestingly, hTERT was detected around the 350-kDa peak (Fraction Nos. B3–B6) concurrently with telomerase activity (Fig. 1B, 1C). Moreover Hsp90 was broadly distributed in two peaks of around 350 kDa and 200 kDa (Fraction Nos. B2–B9). The expression of hTERT by western blotting was higher (mean, five-fold) in HCC tissue than that in cirrhotic nodule tissue (Fig. 1B), and the telomerase activity quantified by TRAP ELISA was significantly higher (>2.5-fold) in HCC than in cirrhotic nodule tissue (Fig. 1B, 1C).

Identification of differentially expressed proteins

To discover hTERT-related proteins, we further analyzed the fractionated lysates of the 350-kDa peak (Fraction No. B4) from HCC and cirrhotic liver tissue by LC-MS/MS. After searching the MASCOT database (http://www.matrixscience.com), 144 proteins were selected according to identification criteria (see Materials and methods), and 24 of all identified proteins displayed more than a two-fold expression difference. Among these 24 proteins, eight were found to be up-regulated in HCC tissue compared with cirrhotic liver tissue, while 16 proteins were found to be down-regulated (Table 1). Of the 24 proteins, nine were already known as HCC-related proteins(14–20). To identify a new prognostic biomarker related to hTERT, we decided to focus on hnRNP A2/B1, which has been reported as a prognostic biomarker for lung cancer(21) and gastric cancer(22).

Validation of heterogeneous nuclear ribonucleoprotein A2/B1 expression and interaction with human telomerase reverse transcriptase subunit

To confirm the altered expression of hnRNP A2/B1 in HCC and non-cancerous liver, western blot analysis was performed with anti-hnRNP A2/B1 antibody. Both of hnRNP A2/B1 expression was detected around 350 kDa (Fraction Nos. B3–B7). The hnRNP A2/B1 protein level was higher in HCC tissue than that in non-cancerous liver tissue (Fig. 2A). To examine whether hnRNP A2/B1 can interact with hTERT, we performed an immunoprecipitation assay. hnRNP A2/B1-immunoprecipitates, derived from fractionated lysates of 350 kDa (Fraction No. B4) contained hTERT (Fig. 2B). However, in a reverse immunoprecipitation experiment, anti-hnRNP A2/B1 antibody was unable to recognize the hTERT protein band in hTERT-immunoprecipitates (data not shown). Therefore, we established Huh7 cells derived from stable cell lines that consistently expressed FLAG-tagged hTERT (see Materials and methods). hnRNP A2/B1-immunoprecipitates contained FLAG-hTERT, and

Table 1. Proteins identified by LC-MS/MS as significantly changed in expression between HCC tissues and cirrhotic nodule tissue[18–24]

Accession no.	Protein name	Molecular function	Protein ratio (HCC/cirrhotioc liver)
Up-regulated proteins in HCC tissue			
P 40925	Malate dehydrogenase	L-malate dehydrogenase activity, malic enzyme activity	2.38
Q 13228	Selenium-binding protein 1	Protein binding, selenium binding	2.07
P 22626	Heterogeneous nuclear ribonucleo protein in A2/B1	RNA binding, nucleotide binding	2.01
Q 13535	Serine/threonine-protein kinase ATR	ATP binding, DNA binding	1.92
Q 5T4S7	Zinc finger UBRl-type protein 1	Ubiquitin-protein in ligase activity, zinc ion binding	1.61
P 07335	Annexin A2	Calcium ion binding, cytoskeletal protein binding	1.53
P 30038	Delta-l-pyrroline-5-carboxylate dehydrogenase	1-pyrroline-5-carboxylate dehydrogenase activity	1.52
P 09651	Heterogeneous nuclear ribonucleo protein A1	RNA binding, nucleotide binding	1.48
Down-regulated proteins in HCC tissue			
Q 8NF91	Nesprin-1	Actin binding, lam in binding	0.67
P 00352	Retinal dehydrogenase 1	Ras GTPase activator activity	0.55
P 24752	Acetyl-coA acetyl transferase	Acetyl-coA acetyl transferase activity	0.51
P 00441	Superoxide dismutase (Cu-Zn)	C haperone binding copper ion binding	0.45
P 02787	Serotransfeirn recursor	Ferric ion binding	0.45
Q 8TE73	Ciliaary dyne in heavy chain 5	ATP binding, ATPase actvity	0.43
P 07327	Alcohol dehydrogenase 1A	Alcohol dehydrogenase activity (Zinc-dependent)	0.41
P 68871	Hemoglobnin subunit beta	Heme binding, hemoglobin binding, oxygen binding	0.39
Q 6PIU 2	Liver carboxyl esterase 1 precursor	Carboxyl esterase activity	0.38
Q 06830	Peroxiredoxin-1	Protein binding,thioredoxin peroxidase activity	0.36
P 69905	Hemoglobin subunit alpha	Heme binding, oxygen binding,	0.34
P 36871	Phosphoglucomutase-1	Magnesium ion binding	0.32
P 05089	Arginase-1	Arginase activity	0.32
P 30041	Peroxiredoxin-6	Glutathione peroxidase activity	0.29
P 00326	Alcohol dehydrogenase 1C	Alcoholdehydrogenase (NAD) activity	0.21
P 08319	Alcohol dehydrogenase 4	NAD binding, NADPH quinone reductase activity	0.15

ATP, adenosine 5'-triphosphate; GTP, guanosine triphosphate; HCC, hepatocellular carcinoma; NAD, nicotinamide adenine dinucleotide; NADPH, nicotinamide adenine dinucleotide phosphate-oxidase.

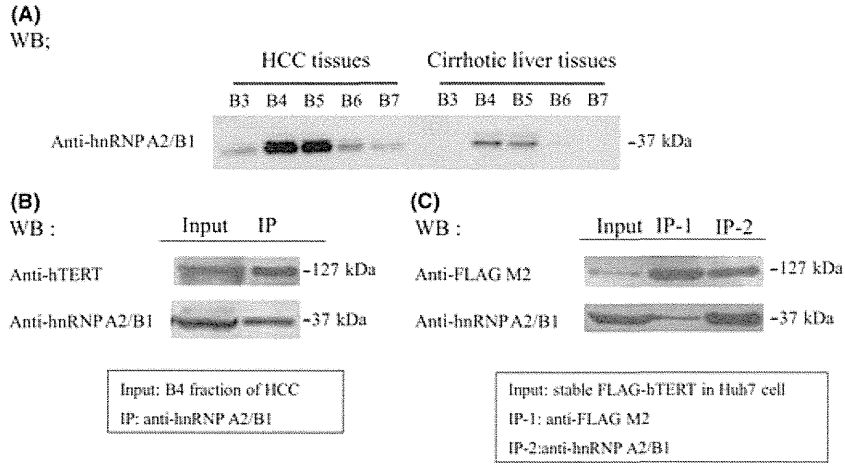

Fig. 2. Validation of hnRNP A1/B2. (A) Representative image of quantitative measurement of hnRNP A2/B1 protein by western blotting with anti-hnRNP A2/B1 antibody. (B) B4 fractionated lysates of HCC were immunoprecipitated with anti-hnRNP A2/B1 antibody. The bound proteins were separated by 8% sodium dodecyl sulfate polyacrylamide gel electrophoresis (SDS-PAGE) and subjected to western blotting with anti-hTERT and anti-hnRNP A2/B1 antibodies as indicated. The B4 fractionated lysates of HCC shown in the input correspond to 5% of the sample. (C) Total cell lysates from Huh7 cells stably expressing FLAG-hTERT were immunoprecipitated with anti-FLAG M2 (IP-1) and anti-hnRNP A2/B1 (IP-2) antibodies. The bound proteins were separated by 8% SDS-PAGE and subjected to western blotting using anti-FLAG M2 and anti-hnRNP A2/B1 antibodies as indicated. Total cell lysates shown in the input correspond to 5% of the sample.

anti-hnRNP A2/B1 antibody recognized the FLAG-hTERT protein band in FLAG-M2 immunoprecipitates (Fig. 2C). These results confirmed that hnRNP A2/B1 can interact with hTERT.

Functional relevance of heterogeneous nuclear ribonucleoprotein A2/B1 expression on telomerase activity

To examine the functional relevance of hnRNP A2/B1 on hTERT activity, we performed knockdown of hnRNP A2/B1. Expression of hnRNP A2/B1 in Huh7 cells was significantly knocked down to 30–40% of the control using hnRNP A2/B1-specific siRNA (siGENOME, Thermo Scientific) (Fig. 3A). Under these conditions, the results of TRAP ELISA showed that telomerase activity was repressed to 43–48% that of the control (Fig. 3B). These results indicate that hnRNP A2/B1 is related to telomerase activity.

Analysis of heterogeneous nuclear ribonucleoprotein A2/B1 expression by immunohistochemistry

To characterize the clinicopathological significance of hnRNP A2/B1 expression in HCC, we performed immunohistochemical staining of hnRNP A2/B1 using paraffin-embedded tumor and non-tumor specimens from 74 HCC patients. We observed hnRNP A2/B1 expression in all HCC specimens, while it was expressed in 16 of 74 (22%) adjacent non-cancerous liver specimens ($P< 0.001$). We did not observe hnRNP A2/B1 expression in normal liver ($n = 5$) or in the early stage (F1–2) of chronic hepatitis ($n = 5$) (data not shown).

Interestingly, we noticed that anti-hnRNP A2/B1 antibody reacted to nuclear and cytoplasmic isoforms of hnRNP A2/B1. We defined HCC cells in which only nuclear hnRNP A2/B1 was expressed in tumor cells as nuclear hnRNP A2/B1-positive HCC (Fig. 4A). Similarly, both nuclear and cytoplasmic hnRNP A2/B1 was expressed in tumor cells as nuclear and cytoplasmic hnRNP A2/B1-positive HCC, respectively (Fig. 4B). Western blotting analysis showed that hnRNP A2/B1 was expressed significantly more, about 2.5-fold, in the nuclear and cytoplasmic hnRNP A2/B1-positive HCC than in the nuclear hnRNP A2/B1-positive HCC Fig. 5A, B).

The expression pattern of hnRNP A2/B1 in the nucleus and the cytoplasm was different in each HCC tissue type. Nuclear hnRNP A2/B1-positive HCC was observed in 40.5% (30 of 74) of HCC patients, whereas nuclear and cytoplasmic hnRNP A2/B1-positive HCC was observed in 59.5% (44 of 74) of HCC patents (Table 2). We then compared the clinicopathological features of nuclear hnRNP A2/B1-positive HCC and nuclear and cytoplasmic hnRNP A2/B1-positive HCC (Table 2). Nuclear and cytoplasmic expression of hnRNP A2/B1 was frequently observed in patients with a progressive histological grading (Edmondson-Steiner grades; $P = 0.002$) and microvascular invasion ($P = 0.013$) (Table 2). No relationship was apparent between the expression pattern of hnRNP A2/B1 and age, gender, type of infected virus, Child-Pugh score, AFP value, PIVKA-II value, tumor size, tumor morphology, TNM stages, or recurrence rate of HCC (Table 2). Importantly, survival analysis using the Kaplan-Meier method revealed that HCC patients with nuclear and cytoplasmic expression of hnRNP A2/B1 showed a significant lower survival rate than those with nuclear expression of hnRNP A2/B1 (log-rank test, $P = 0.0027$; Fig. 6). Furthermore, univariate Cox regression analysis showed that nuclear and cytoplasmic expression of hnRNP A2/B1 was significantly associated with low patient survival (HR, 2.37; 95% CI, 1.33–4.23;

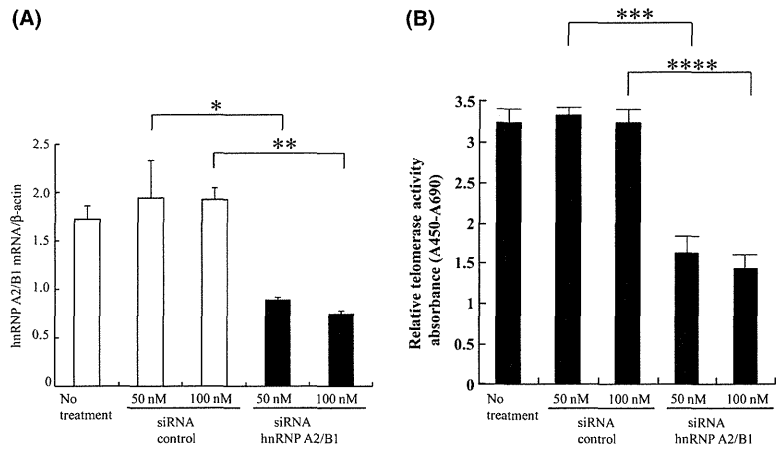

Fig. 3. siRNA against hnRNP A2/B1 suppresses telomerase activity. (A) mRNA expression of hnRNP A2/B1 after small interfering (si)RNA transfection in Huh7 cells transfected with sihnRNP A2/B1 and that of control siRNAs. Levels of mRNA were determined by real time polymerase chain reaction (PCR). (B) The activity of each lysate was determined by TRAP ELISA (*,**,***,****$P < 0.05$).

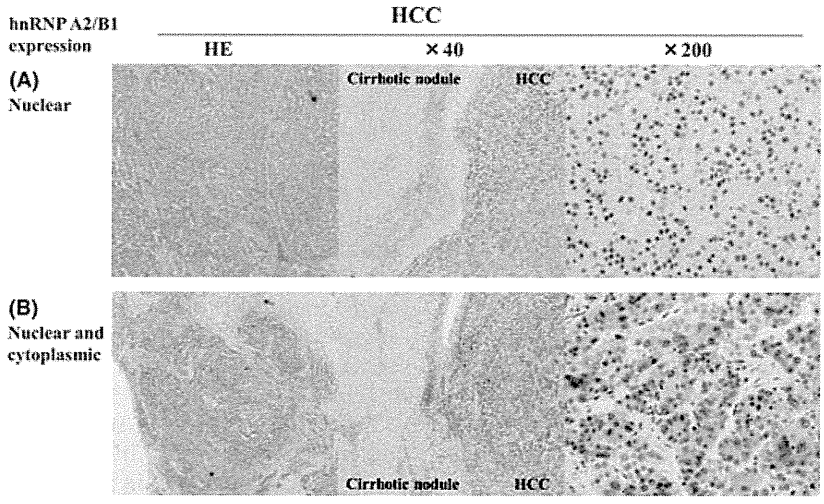

Fig. 4. Immunohistochemical analysis of hnRNP A2/B1 expression in HCC and adjacent cirrhotic liver tissue. A representative photomicrograph of hematoxylin and eosin staining and hnRNP A2/B1 staining in HCC tissue (× 40 and × 200, respectively) and adjacent cirrhotic liver tissue (× 40). (A) Nuclear hnRNP A2/B1-positive HCC. (B) Nuclear and cytoplasmic hnRNP A2/B1-positive HCC.

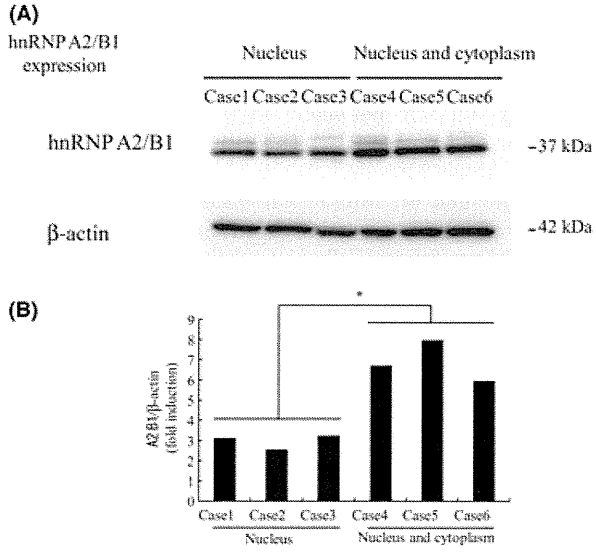

Fig. 5. The protein expression of hnRNP A1/B2 in HCC tissue. (A) Equal amounts of HCC tissue from Nuclear hnRNP A2/B1-positive HCC (cases 1–3) and Nuclear and cytoplasmic hnRNP A2/B1-positive HCC (cases 4–6) were loaded into the SDS-PAGE gel and normalized by comparing with β-actin. (B) The value in the graph is presented as mean ± SD (*$P < 0.05$).

$P = 0.004$) (Table 3). Multivariate Cox regression analysis showed that nuclear and cytoplasmic expression of hnRNP A2/B1 was an independent prognostic factor associated with low patient survival (HR, 3.86; 95% CI, 1.80–8.28; $P = 0.001$). Other clinicopathological features did not add independent prognostic information in this study (Table 3). These results demonstrate that

Table 2. Clinicopathological characteristics and hnRNP A2/B1 expression of nucleus (&) cytoplasm in HCC ($n = 74$)

hnRNP A2/B1 expression	nuclear (n=30)	nuclear and cytoplasm ic (n=44)	P-value
Age (<60 years/ ≥ 60 years)	12/18	18/26	0.938
Gender (male/female)	22/8	18/26	0.531
Virus (HBV/HCV/NBNC)	5/21/4	14/21/9	0.160
Child-Pugh (5/6/7)	28/2/0	37/5/2	0.377
AFP (<100 ng/ml/ ≥ 100 ng/ml	20/10	26/18	0.509
PIVKA-II (<100 mAU/ml/ ≥ 100 mAU/ml	18/12	22/22	0.397
Histological grading (well/moderately/poorly)	12/18/0	0/32/12	0.002
Tumor size (<3 cm/ ≥ 3 cm)	16/14	22/22	0.778
Tumor morphology (uni/multi)	26/4	35/9	0.429
TMN classification (I/II/III/IVa)	6/17/6/1	2/27/10/5	0.139
Microvascular invasion (Yes/No)	11/19	29/15	0.013
HCC recurrence (Yes/No)	11/19	20/24	0.452

AFP, α-fetoprotein; HBV, Hepatitis B virus; HCC, hepatocellular carcinoma; HCV, Hepatitis C virus.

the expression of hnRNP A2/B1 correlates with the severity and progression of HCC and that nuclear and cytoplasmic hnRNP A2/B1 expression could be a useful biomarker for predicting the survival of HCC patients after surgical resection.

Discussion

The development of useful biomarkers for the early detection and prediction of HCC is urgently required to improve prognosis of patients with HCC. Moreover,

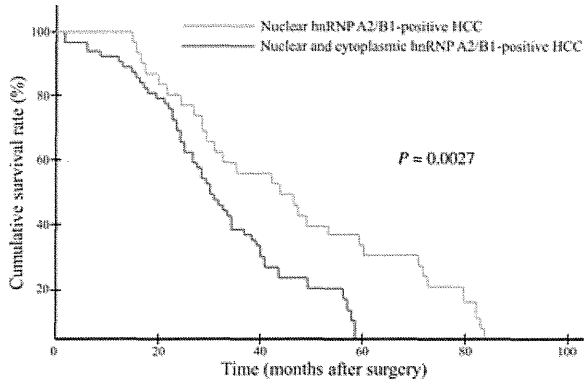

Fig. 6. Kaplan-Meier survival analysis of nuclear (and) cytoplasmic hnRNP A2/B1-positive HCC (log rank test).

biomarkers reflecting malignant features of HCC might be useful for the following patients and HCC therapy selection since HCC relapse frequently occurs in residual liver where HCC has been curatively removed by surgical treatment. Although AFP and PIVKA II are reliable tumor markers for the detection of recurrence of HCC, more than 50% of patients with small HCC (<2 cm) test negative for these markers(23).

A two-dimensional electrophoresis and mass spectrum-based proteomic strategy provide high-throughput simultaneous identification of hundreds of proteins; such a strategy is considered very valuable for screening tumor biomarkers(24, 25). Here, we applied a different approach for identifying telomerase-associated proteins in this study. According to previously reported methods (12), protein lysates of HCC tissue and non-cancerous tissue were subjected to HPLC gel filtration. A previous study using a soluble fraction of Huh7 cells identified two peak of endogenous hTERT at around 680 kDa and 350 kDa (data not shown). It was speculated that a dimer form of hTERT existed in the 680 kDa peak and a monomer in the 350 kDa peak. Hsp90 was exclusively distributed in the 350 kDa peak but not in the 680 kDa peak (data not shown). Unlike previous studies using Huh7 cells, we could not detect the 680 kDa peak fraction in HCC tissue. We could however detect the 350 kDa peak and the 200 kDa peak fraction in HCC tissue. The telomerase complex existed in the 350 kDa peak fraction. Moreover, Hsp90 existed in 350 kDa peak fraction, while many of the metabolic-related proteins were identified in the 200 kDa peak fraction. These data suggest that hTERT-associated proteins might exist in the 350 kDa peak fraction in HCC tissue.

Further analysis of the fractionated lysates of 350 kDa by LC-MS/MS revealed that 24 proteins were differentially expressed in HCC tissue when compared with nontumor tissue. In addition, 9 of the 24 proteins were already known as HCC-related proteins(14–20). We therefore focused on hnRNP A2/B1, one of the most abundant and important nuclear RNA-binding proteins involved in packaging nascent mRNA, alternative splicing(26, 27) and cytoplasmic RNA trafficking(28), translation(29), and stabilization(30).

To our knowledge, this is the first demonstration of hnRNP A2/B1 interaction with hTERT by immunoprecipitation *in vitro* and *in vivo*. hnRNP A2/B1 acts as a molecular adapter between single-stranded telomeric repeats or telomerase RNA (hTERC), and another segment of single-stranded DNA(31, 32). However the details for such an interaction need further investigation. Of the telomerase-related proteins, Hsp90 has been shown to be a functionally critical factor for telomerase activity *in vivo* and *in vitro*(33). The telomerase complex with Hsp90 within the 350 kDa complex was also detected in this study, confirming the biological functionality of telomerase activity (Fig. 1B,C). Hsp90 inhibitors reduce the amount of hTERT as well as telomerase activity(12). Despite the concentration of Hsp90

Table 3. Cox regression analysis of cumulative survival rate relative to nuclear and cytoplasmic hnRNP A2/B1 expression and clhicopathobgical parameters of primary HCC patients (*n*=74)

	Univariate		Mulivarate	
Variables	HR (95%CI)	*P*-value	HR (95%CI)	*P*-value
Age ≥ 60 years	1.25 (0.74–2.11)	0.453		
Male gender	1.16 (0.69–2.05)	0.606		
Child-Pugh ≥ 6	1.01 (0.36–2.84)	0.979		
AFP ≥ 100 ng/ml	1.42 (0.84–2.41)	0.188	1.25 (0.72–2.18)	0.429
PIVKA-II ≥ 100 mAU/ml	1.44 (0.85–2.45)	0.171	1.05 (0.59–1.90)	0.864
Histological grade (poorly)	1.33 (0.60–2.96)	0.485		
Tumorisize ≥ 3 cm	1.37 (0.83–2.25)	0.225		
Tumor morphology (multi)	1.09 (0.57–2.06)	0.797		
TMN cfessificaton (III, IVa)	1.63 (0.89–2.96)	0.112	1.24 (0.65–2.36)	0.51
Microvascular invasion (Yes)	1.08 (0.65–1.79)	0.765		
HCC recurrence (Yes)	0.73 (0.44–1.23)	0.238		
Nuclear and cytoplasmic hnRNP A2/B1	2.37 (1.33–4.23)	0.004	2.18 (1.19–4.00)	0.012

AFP, α-fetoprotein; HCC, hepatocellular carcinoma.

inhibitors, no telomere shortening of Hsp90 inhibitor-treated cells was observed (data not shown). The present study also demonstrated that the suppression of hnRNP A2/B1 by siRNA inhibited telomerase activity *in vitro*. However, unlike Hsp90, the suppression of hnRNP A2/B1 could potentially shorten telomere length and inhibit cell proliferation, although such an hypothesis should be confirmed by further experiments.

To further examine the clinicopathological significance of hnRNP A2/B1, immunohistochemical staining in clinical HCC samples was performed. Both nuclear and cytoplasmic expression of hnRNP A2/B1 in HCC was significantly related to tumor differentiation and microvascular invasion of HCC (Table 2). Furthermore survival analysis showed a significant correlation between the high nuclear and cytoplasmic expression of hnRNP A2/B1 in HCC and the low survival rate of patients (Table 3, Fig. 6). Although high nuclear and cytoplasmic expression of hnRNP A2/B1 in HCC was not associated with the recurrence rate of HCC (Tables 2, 3), it was associated with the recurrence pattern of HCC. Tumor morphology (multiple HCCs; $P = 0.100$) and vascular invasion ($P = 0.070$) in recurrence was observed more frequently in patients with nuclear and cytoplasmic hnRNP A2/B1-positive HCC than in those with nuclear hnRNP A2/B1-positive HCC, although the difference was not statistically significant (data not shown). The metastatic and invasive features of HCC with nuclear and cytoplasmic expression of hnRNP A2/B1 may contribute to the poor prognosis of affected patients.

Because hnRNP A2/B1 is a RNA shuttling factor(34), nuclear and cytoplasmic expression patterns might reflect increased hnRNP A2/B1 in cells; however, the expression of hTERT is presumably increased and colocalized with hnRNP A2/B1. It was reported that nucleolin, a molecule shuttling into and out of the nucleus, mediates hTERT and localization of hTERT shifted from the nucleus to the cytoplasm depending on its sublocalization(35). Increased hTERT might be associated with tumor differentiation, microvascular invasion and survival of HCC.

While preparing this study, Cui H. *et al.*(36) reported similar findings. They showed increased localization of hnRNP A2/B1 in the cytoplasm of HCC cells during dedifferentiation of HCC. Our study, however, showed the functional relevance of hnRNP A2/B1 on telomerase activity and demonstrated the clinical importance of hnRNP A2/B1 for patient survival.

In conclusion, employing a proteomic screening and molecular biology verification approach revealed a potential HCC biomarker, hnRNP A2/B1, and confirmed its usefulness in the diagnosis of and prediction of prognosis of HCC. Although the present data suggest that hnRNP A2/B1 is clinically significant, the understanding of its underlying mechanisms falls short of that required for the development of practical applications. Further approaches are thus needed to improve the diagnostic performance of hnRNP A2/B1 for biological and clinical detection of HCC.

Acknowledgements

We thank M. Baba, N. Nishiyama, and Y. Fujita for their technical assistance, and Drs. Y Hinoue, S Aoyama, and K Minouchi at Toyama City Hospital for their help with clinical support.

References

1. Thorgeirsson SS, Grisham JW. Molecular pathogenesis of human hepatocellular carcinoma. *Nat Genet* 2002; **31**: 339–46.
2. Parkin DM, Bray F, Ferlay J, Pisani P. Global cancer statistics. *CA Cancer J Clin* 2005; **55**: 74–108.
3. de Lange T. Ending up with right partner. *Nature* 1998; **392**: 753–54.
4. Blackburn EH. Telomere states and cell fates. *Nature* 2000; **408**: 53–6.
5. Bodnar AG, Ouellette M, Frolkis M, *et al.* Extension of life-span by introduction of telomerase into normal human cells. *Science* 1998; **279**: 349–52.
6. Feng J, Funk WD, Wang SS, *et al.* The RNA component of human telomerase. *Science* 1995; **269**: 1236–41.
7. Weinrich SL, Pruzan R, Ma L, *et al.* Reconstitution of human telomerase with the template RNA component hTR and the catalytic protein subunit hTRT. *Nat Genet* 1997; **17**: 498–502.
8. de Lange T. Protection of mammalian telomerase. *Oncogene* 2002; **21**: 532–40.
9. Yan P, Benhattar J, Seelentag W, Stehle JC, Bosman FT. Immunohistochemical localization of hTERT protein in human tissues. *Histochem Cell Biol* 2004; **121**: 391–7.
10. Desmet VJ, Gerber M, Hoofnagle JH, Manns M, Scheuer PJ. Classification of chronic hepatitis: diagnosis, grading and staging. *Hepatology* 1994; **19**: 1513–20.
11. Shirota Y, Kaneko S, Honda M, Kawai FH, Kobayashi K. Identification of differntially expressed genes in hepatocellular carcinoma with cDNA microarrays. *Hepatology* 2001; **33**: 832–40.
12. Mizuno H, Khurts S, Seki T, *et al.* Human telomerase exists in two distinct active complexes *In Vivo*. *J Biochem* 2007; **141**: 641–52.
13. Masutomi K, Yu EY, Khurts S, *et al.* Telomerase maintains telomere structure in normal human cells. *Cell* 2003; **114**: 241–53.
14. Kim SY, Lee PY, Shin HJ, *et al.* Proteomic analysis of liver tissue from HBx-transgenic mice at early stages of hepatocarcinogenesis. *Proteomic* 2009; **22**: 5056–66.
15. Sun W, Xing B, Sun Y, *et al.* Proteomic analysis of hepatocellular carcinoma by two-dimensional difference gel electrophoresis. *Mol Cell Proteomics* 2007; **6**: 1798–808.
16. Mohammad HS, Kurikihchi K, Yoneyama H, *et al.* Annexin A2 expression and phosphorylation are up-regulated in hepatocellular carcinoma. *Int J Oncol* 2008; **33**: 1157–63.
17. Liang CRM, Leow CK, Neo JCH, *et al.* Proteomic analysis of human hepatocellular carcinoma tissues by two-dimensional difference gel electrophoresis and mass spectrometry. *Proteomics* 2005; **5**: 2258–71.